

This volume is the property of the University of Oklahoma, but the literary rights of the author are a separate property and must be respected. Passages must not be copied or closely paraphrased without the previous written consent of the author. If the reader obtains any assistance from this volume, he must give proper credit in his own work.

I grant the University of Oklahoma Libraries permission to make a copy of my thesis upon the request of individuals or libraries. This permission is granted with the understanding that a copy will be provided for research purposes only, and that requestors will be informed of these restrictions.

NAME _____

DATE _____

A library which borrows this thesis for use by its patrons is expected to secure the signature of each user.

This thesis by HENRY BADRA has been used by the following persons, whose signatures attest their acceptance of the above restrictions.

NAME AND ADDRESS

DATE

FIELD CHARACTERIZATION AND ANALOG MODELING OF NATURAL FRACTURES IN THE WOODFORD SHALE, SOUTHEAST OKLAHOMA

UNIVERSITY OF OKLAHOMA
GRADUATE COLLEGE

A THESIS APPROVED FOR THE
CONOCOPHILLIPS SCHOOL OF GEOLOGY AND GEOSPATIAL
FIELD CHARACTERIZATION AND ANALOG MODELING OF NATURAL
FRACTURES IN THE WOODFORD SHALE, SOUTHEAST OKLAHOMA

A THESIS

SUBMITTED TO THE GRADUATE FACULTY

in partial fulfillment of the requirements for the

Degree of

MASTER OF SCIENCE

[Faint signatures and names of faculty members]
Dr. Roger Alan Cook
Dr. [unclear]
Dr. [unclear]

By

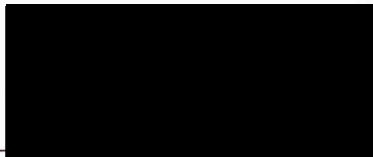
HENRY BADRA
Norman, Oklahoma
2011

00
THESIS
BAD
cop.3

FIELD CHARACTERIZATION AND ANALOG MODELING OF NATURAL
FRACTURES IN THE WOODFORD SHALE, SOUTHEAST OKLAHOMA

A THESIS APPROVED FOR THE
CONOCOPHILLIPS SCHOOL OF GEOLOGY AND GEOPHYSICS

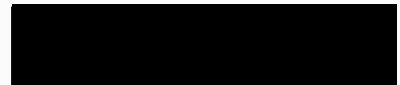
BY



Dr. Roger Slatt, Chair



Dr. Neil Suneson



Dr. Ze'ev Reches

ACKNOWLEDGEMENTS

I would like to thank my academic advisor Dr. Roger M. Slatt for all his support throughout my Masters and for providing me with great experiences and opportunities. I would like to thank Dr. Neil Suneson for encouraging me to pursue a PhD-related study and also Dr. Fa'ez Ratches for providing key insights and support for experimental research. I would like to thank Dr. Shankar Mitra for his access to the Physical Modeling Laboratory.

I would like to acknowledge Devon Energy and Dr. Roger Slatt for providing funding for this thesis. I would like to acknowledge the landowners of Vines Beam and Lazy S Ranch for allowing me access to their property to conduct fieldwork. I would like to thank Bob Allen of Ardmore, Oklahoma, who provided assistance and arranged access to field locations. I would like to thank Jefferson Chang for developing an image analysis program for MatLab.

I would like to extend my gratitude to Rogerick Perez and Oswaldo Davogualdo who helped with fieldwork and securing access to field locations. I also would like to express my appreciation to Paul Deshpande for helpful insight and discussion on aging modeling and fracturing.

I would like to extend my gratitude to my family and friends for their love and support.

ACKNOWLEDGEMENTS

I would like to thank my academic advisor Dr. Roger M. Slatt for all his support throughout my Master's and for providing me with great experiences and opportunities. I would like to thank Dr. Neil Suneson for encouraging me to pursue a field-based study and also Dr. Ze'ev Reches, for providing key insights and support for experimental research. I would like to thank Dr. Shankar Mitra for the access to the Physical Modeling Laboratory.

I would like to acknowledge Devon Energy and Dr. Roger Slatt for providing funding for this thesis. I would like to acknowledge the landowners of Vines Dome and Lazy S Ranch for allowing me access to their property to conduct fieldwork. I would like thank Bob Allen of Ardmore, Oklahoma, who provided assistance and arranged access to field locations. I would like to thank Jefferson Chang for developing an image analysis program for MatLab.

I would like to extend my gratitude to Roderick Perez and Oswaldo Davogustto who helped with fieldwork and securing access to field locations. I also would like to express my appreciation to Paul Debapriya for helpful insight and discussion on analog modeling and fracturing.

Lastly I would like to extend my gratitude to my family and friends for their endless support.

TABLE OF CONTENTS

ACKNOWLEDGEMENTS.....	IV
TABLE OF CONTENTS.....	V
LIST OF TABLES.....	VII
LIST OF FIGURES.....	VIII
ABSTRACT.....	XIII
1. INTRODUCTION.....	1
1.1 OBJECTIVES.....	2
1.2 PREVIOUS WORK.....	3
1.3 GEOLOGY OF THE STUDY AREA.....	7
1.3.1 STRUCTURAL OVERVIEW OF THE ARBUCKLE MOUNTAINS.....	9
1.3.2 STRATIGRAPHIC OVERVIEW OF THE STUDY AREA.....	11
1.4 FRACTURES.....	18
1.4.1 FAILURE.....	19
1.4.2 PRINCIPAL STRESSES.....	20
1.4.3 LAYERS.....	21
2. ANALOG MODELING.....	22
2.1 METHODS.....	22
2.2 RESULTS.....	28
2.3 DISCUSSION.....	32
3. FIELD WORK.....	34
3.1 METHODS.....	34
3.1.1 OUTCROP DESCRIPTIONS.....	36
3.1.2 FRACTURE ANALYSIS.....	36
3.2 RESULTS.....	38
3.2.1 OUTCROP LITHOFACIES.....	38
3.2.2 OUTCROP FRACTURES TYPES.....	40
3.2.3 VINES CREEK.....	43

3.2.4 COOL CREEK (LAZY S RANCH).....	50
3.2.5 OKLAHOMA HIGHWAY 77D.....	55
3.3 DISCUSSION.....	58
3.3.1 GAMMA-RAY AND SEQUENCE STRATIGRAPHY.....	58
3.3.2 FRACTURE MAPPING.....	59
3.3.3 FRACTURES AND MECHANICAL STRATIGRAPHY.....	62
3.3.4 APPLICATION FOR DRILLING AND COMPLETION.....	65
4. CONCLUSIONS.....	68
5. RECOMMENDATIONS.....	71
REFERENCES.....	72

LIST OF TABLES

Table 1 Setup of the analog models.....	24
Table 2 Outcrop lithofacies classification from the Woodford Shale outcrops.....	38
Table 3 Outcrop fracture classification from the Woodford Shale outcrops.....	40

LIST OF FIGURES

Figure 1 Wyche Shale pit fracture orientations obtained from scan lines on the outcrop floor and LIDAR on outcrop walls (Portas, 2009).....	3
Figure 2 Wyche Shale pit electric, mineralogical and borehole image logs (Slatt et al., 2011).....	4
Figure 3 Relationship of fracture density to mechanical unit thickness from Woodford Shale outcrops throughout the Arbuckle Mountains (Ataman, 2008).	5
Figure 4 Models for fracture formation in brittle/ductile rocks (Busetti, 2009).	6
Figure 5 Arbuckle Mountains outline with major faults and folds. Study locations: 1) Oklahoma Highway 77D road cut 2) Vines Creek 3) Cool Creek; modified from Ham (1969).....	7
Figure 6 Geologic map of the study area. Outcrop locations: 1) Oklahoma Highway 77D 2) Vines Creek 3) Cool Creek. Measured orientations shown on rose diagrams (modified from Oklahoma Water Resources Board map viewer, 2011).....	8
Figure 7 Maximum principal stress orientation northeast-southwest derived from borehole breakouts from Heidback et al. (2008).....	10
Figure 8 Stratigraphy for the Paleozoic section in the study area; modified from Ham et al. (1964).....	11
Figure 9 Woodford Shale outcrop with interbedded chert and laminated siltstone.....	15

Figure 10 Woodford Shale members as described in electric logs, lithofacies, depositional environment (modified from Cardott, 2007 and Slatt et al., 2011).....	16
Figure 11 Fracturing modes: Mode I extension, Mode II sliding, Mode III tearing (Ataman, 2008).....	18
Figure 12 Apparatus used for analog modeling experiments. The clay and Play-Doh models were mounted on the latex sheet.....	23
Figure 13 Setup for experiment 1: Play-Doh extensional (not to scale).....	25
Figure 14 Setup for experiment 2: Play-Doh/clay extensional deformation (not to scale).....	25
Figure 15 Setup for experiment 3: Play-Doh/clay/Play-Doh extensional deformation (not to scale).....	26
Figure 16 Setup for experiment 4: clay/Play-Doh/clay extensional deformation (not to scale).....	27
Figure 17 Setup 1 showing a single sheet of ductile Play-Doh after extension.	28
Figure 18 Setup 2 showing a ductile Play-Doh layer (bottom) and a brittle clay layer (top) after extension. Early stage tensile fractures (red). Inclined shear fractures (blue) seen on the side and top of the clay.....	28
Figure 19 Top and side view of Setup 2 showing progression of fracturing in the early, middle and late stage of the experiment.....	29
Figure 20 Setup 3 showing a ductile Play-Doh layer (bottom), a brittle clay layer (middle), and a ductile Play-Doh (top) after extension. Short fractures are seen on the side of the clay layer.....	30

Figure 21 Setup 4 showing a brittle clay layer (bottom), a ductile Play-Doh layer (middle), and a brittle clay layer (top) after extension. Fractures are seen on the side of the clay layers.....31

Figure 6 Scintrex GRS-500 hand-held detector used to create outcrop gamma-ray logs.....35

Figure 23 Woodford Shale outcrop lithofacies. A. Calcareous mudstone B. Laminated siltstone C. Chert D. Phosphatic mudstone E. Laminated organic-rich claystone.....39

Figure 24 Woodford Shale outcrop fracture types. A. Stratabound B. Layer-cutting angled C. Layer-cutting jagged D. Curved E. Swarming F. Faults. Images A-C were taken perpendicular to the orientation of bedding planes. Images D-F were taken parallel to the orientation of bedding planes.....42

Figure 25 Vines Creek Woodford Shale outcrop of north-dipping beds, looking west.....43

Figure 26 Vines Creek graphical relationship between bed thickness and joint spacing for the stratabound fracture type.....44

Figure 27 Vines Creek fracture survey square completed from outcrop exposures. Prominent bed boundaries are shown as horizontal lines. Lithofacies present include chert and laminated siltstone. Stratabound fractures are shown as short lines perpendicular to bedding in chert. Layer-cutting angled fractures are dashed and present in laminated siltstone. The image is oriented west to east.....45

Figure 28 Vines Creek fracture directions.....46

Figure 29 Vines Creek outcrop gamma-ray log, with typical rock characteristics.....47

Figure 30 Vines Creek outcrop gamma-ray and spectral gamma-ray logs. Log patterns are highlighted.....	48
Figure 31 Cool Creek Woodford Shale outcrop.....	50
Figure 32 Cool Creek fracture orientations.....	51
Figure 33 Cool Creek fracture survey square completed from outcrop exposures. Prominent bed boundaries are shows as vertical lines. Lithofacies present include chert and calcareous mudstone Stratabound fractures are shown as short lines perpendicular to bedding in chert beds. Layer-cutting jagged fractures are dashed and cut across different lithofacies.....	52
Figure 34 Cool Creek fracture survey square completed from outcrop exposure. Prominent bed boundaries are shows as vertical lines. Stratabound fractures are shown as short lines perpendicular to bedding. Layer-cutting fractures are dashed and angled to bedding.....	53
Figure 35 Cool Creek graphical relationship between bed thickness and fracture spacing.....	54
Figure 36 Oklahoma Highway 77D Woodford Shale outcrop of overturned beds, view is to the north.....	55
Figure 37 Oklahoma Highway 77D fracture orientations.....	56
Figure 38 Oklahoma Highway 77D fracture survey square completed from outcrop exposures. Map constructed from laminated siltstone bedding plane shows layer-cutting angled fractures as short lines. Faults are dashed, segmented and offset other fractures. Clay gouge is present along the faults..	57
Figure 39 Vines Creek outcrop gamma-ray correlated with Henryhouse Creek Woodford Shale outcrop from Krystyniak (2006).....	58

Figure 40 Failure mode relationships to principal stresses (Cosgrove, 2001)...63

Figure 41 Comparison of typical Woodford Shale outcrop section and results from Setup 3 analog modeling of brittle-ductile couplets.....64

ABSTRACT

Understanding the mechanisms under which shales deform is fundamental to improving exploration success in unconventional resource plays. Several outcrops of the Woodford Shale have been chosen to characterize fracture patterns at the outcrop level and relate them to the principal stresses of the of the study area and rock types of the formation. The outcrops are located in the Arbuckle Mountains of Oklahoma. This region is composed of several northwest-trending folds and regional fault systems. Excellent outcrop exposures of the Woodford Shale are used as reservoir analogs.

Field analysis consisted of outcrop gamma-ray logs, facies descriptions and fracture characterization. Key interpretations include: 3rd order sea level cycles from gamma-ray parasequences, five distinct lithofacies, and abundant natural tensile fractures.

Alternating sequences of laminated claystone and siltstone are rich in organic content and are mechanically ductile. Bedded chert is less organic rich, and mechanically brittle. Therefore, the Woodford Shale can be defined as an axially anisotropic material in the direction perpendicular to the bedding and an isotropic material in the direction parallel to the bedding. Fractures were observed in the field to be planar and perpendicular to bedding in cherts, and inclined with respect to bedding in laminated clay-rich layers.

A simple analog model constructed with a layered sequence of Play-Doh and clay was used to examine the relationship between alternating brittle/ductile

sequences and the development of fractures. The conclusions of these experiments are: 1) laminations in shale formations can be an important control on the propagation of natural fractures and 2) fracture patterns in shales are broadly predictable based on the correct identification of brittle and ductile layers using gamma-ray logs. Decreasing gamma-ray and spectral gamma-ray log patterns may indicate brittle zones which would be most favorable for horizontal-well placement and fracture stimulation. Zones with high gamma-ray and high levels of uranium may be problematic for horizontal drilling due to likelihood of higher clay content and may serve as fracture stimulation barriers.

1. INTRODUCTION

Horizontal drilling and hydraulic fracturing have revolutionized development of unconventional shale plays. These engineering techniques require increasing knowledge of the geology of unconventional reservoirs in order to improve efficiency and results. Research into the various lithofacies, geochemistry, and mechanical properties of mudstones has become influential in the elevated interest in unconventional shale plays by the energy industry.

Natural fractures are very important in unconventional shale plays because they provide insight into the mechanical behavior of the lithofacies. Pre-existing fractures in shales can be mineralized and create planes of weakness in the rock. Natural fractures also provide key indications of earth stresses. These pre-existing planes of weakness can also be fluid-filled and provide pore space and pathways for subsurface fluids. In turn, high fracture permeability can also lead to riskier targets for oil and gas exploration as water can easily migrate along fracture swarms. Understanding how layered material deforms is also essential in the production effort of man-made fracture networks. The key to successful development of these complex reservoirs will be heavily influenced by understanding how natural failure has occurred in layered, low-permeability, organic-rich lithofacies.

The University Of Oklahoma Institute of Reservoir Characterization conducts numerous qualitative and quantitative analyses that characterize prominent midcontinent shale formations. The characterization of the Devonian

Woodford Shale is of particular interest due to the proximity of field locations and the direct application of research to ongoing exploration and production by energy companies.

1.1 Objective

The objective of further characterizing fractures in the field is to gain a better understanding of the relationships between stratigraphy and fractures. These relationships have been a topic of interest for long time (Reches, 1983; Engelder, 1987; Gross, 1995; Hudson et al., 1996; Ataman, 2008; Buseti, 2009). These studies are further expanded here by using analog laboratory models to simulate processes of natural fracturing in brittle/ductile materials.

The specific goals of this study are to: 1) characterize the Woodford Shale in outcrop with total and spectral gamma-ray logs 2) describe the lithofacies and measure fracture orientations; 3) establish the role of laminations in fracture propagation; 4) develop a conceptual structural model to help explain the fracturing process in layered strata.

It is expected that the results will provide new knowledge to help: 1) identify potential exploration sweet spots in unconventional shales by predicting spatial and stratigraphic areas of higher fracture density, and 2) improve the placement of hydraulic fractures in shales through understanding of natural fracture propagation.

1.2 Previous Work

In a previous study, Portas (2009) characterized the general large-scale fracture patterns in the Woodford Shale (Figure 1). This study took place in the Wyche Shale pit near the Arbuckle Mountains in south-central Oklahoma and the results were correlated with a nearby well.

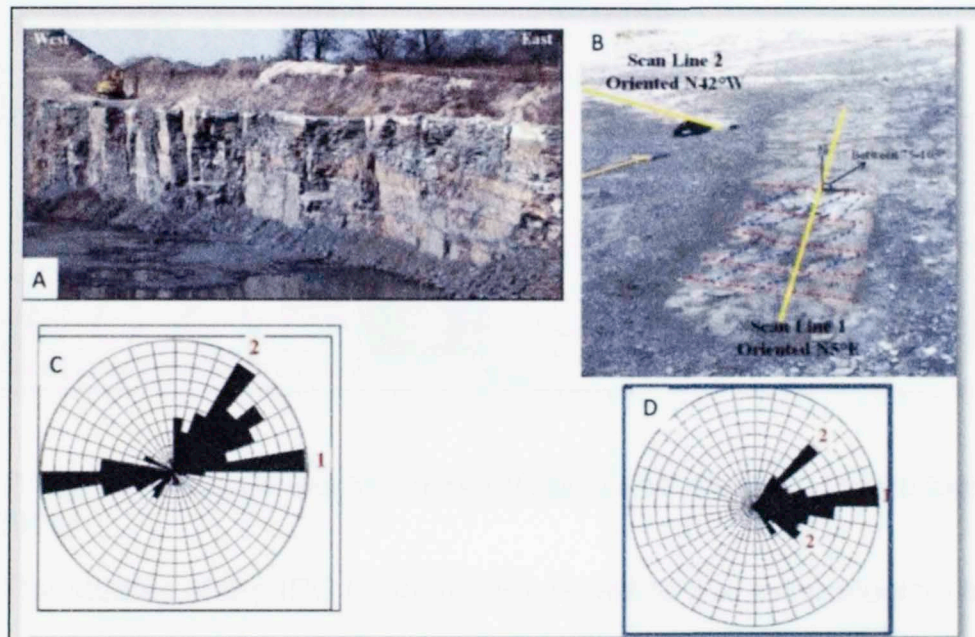


Figure 1 Wyche Shale pit fracture orientations obtained from scan lines on the outcrop floor and LIDAR on outcrop walls (Portas, 2009).

Portas (2009) demonstrated the application of LIDAR for analysis of large scale fracturing in outcrops. As part of an ongoing research project, 2D seismic lines were also obtained on the outcrop, which showed faulting, and the boundary unconformity between the Woodford Shale and the underlying Hunton Group.

Stratigraphic, geochemical and geomechanical properties of the Woodford Shale were characterized at various scales from core analysis

(Miccelli, 2010; Sierra et al. 2010; Slatt and Abousleiman, 2011). Studies are currently underway or have been recently completed by members of the Institute of Reservoir Characterization (IRC) on these subjects (Slatt et al., 2011).

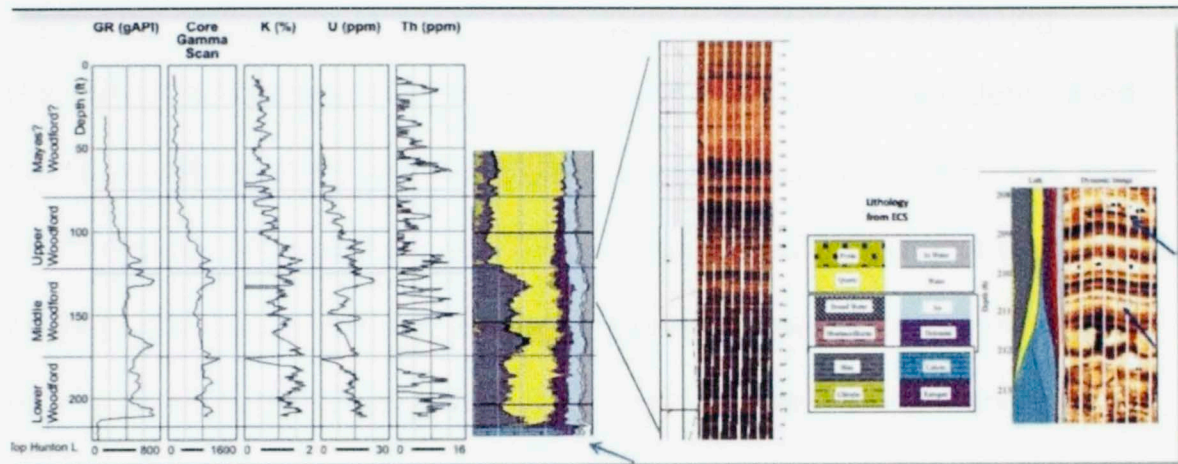


Figure 2 Wyche Shale pit electric, mineralogical and borehole image logs (Slatt et al., 2011)

The studies of the IRC have already revealed that mineralogical and geochemical changes through the formation greatly influence the mechanical properties of the Woodford Shale. This workflow (Figure 2) also demonstrated a technique for identifying the mechanical properties of mudstones from the reservoir to the nano-scale (Slatt et al. 2011). Analysis of the mechanical properties of the Woodford Shale from Wyche Pit provided the basis for this investigation. Sierra et al. (2010) identified a traverse isotropy to the Poisson's ratio and Young's Modulus as a result of layers in the lithofacies of the Woodford Shale. The layering in the Woodford Shale is pervasive at all scales, making the formation a mechanically anisotropic material in the direction normal to bedding.

Other field-based projects completed at Oklahoma State University by Krystyniak (2006) and Ataman (2008) established a relationship between outcrop gamma-ray patterns and subsurface-log responses, and presented key findings on the nature of fractures in the Woodford Shale. Ataman (2008) observed a general trend of decreasing fracture density with increasing mechanical unit thickness for the Woodford Shale (Figure 3) and determined that micro fractures tend to be parallel to bedding. However, brittle beds have more fractures perpendicular to bedding. Krystyniak (2006) used a relationship between gamma-ray and sea-level changes and applied it to determining the sequence stratigraphic relationship of several Woodford Shale outcrops.

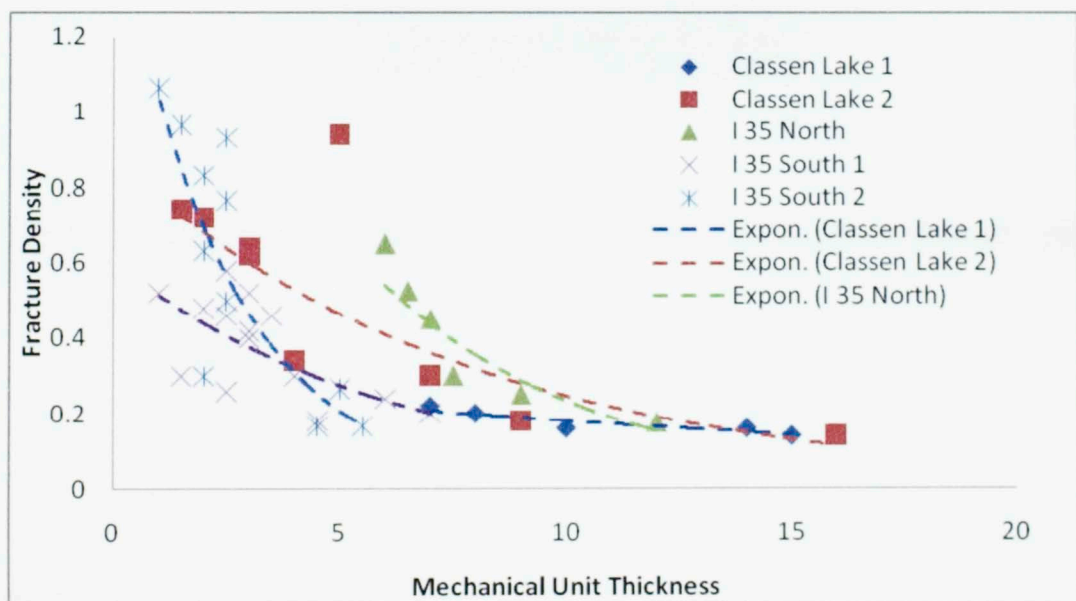


Figure 3 Relationship of fracture density to mechanical unit thickness from Woodford Shale outcrops throughout the Arbuckle Mountains (Ataman, 2008).

Busetti (2009) completed a Ph.D. dissertation at the University of Oklahoma on the subject of fracture mechanics in sedimentary rocks, and presented a basis for analysis of brittle-ductile rocks in the field (Figure 4). This study resulted in conclusions that brittle layers contained more fractures. Also, that a weak correlation exists between fracture spacing and layer thickness. Lastly, the proximity to faults and flexures can relate to areas of high density fracturing.

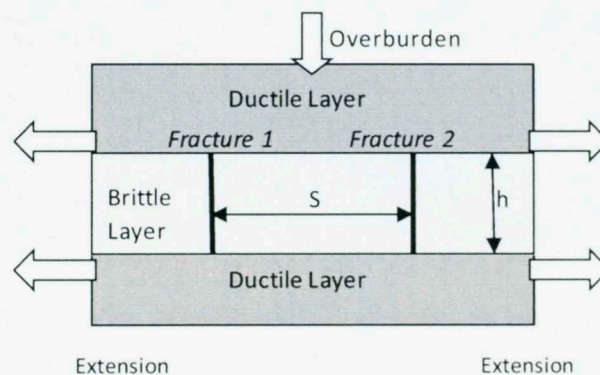


Figure 4 Models for fracture formation in brittle/ductile rocks (Busetti, 2009).

1.3 Geology of the study area

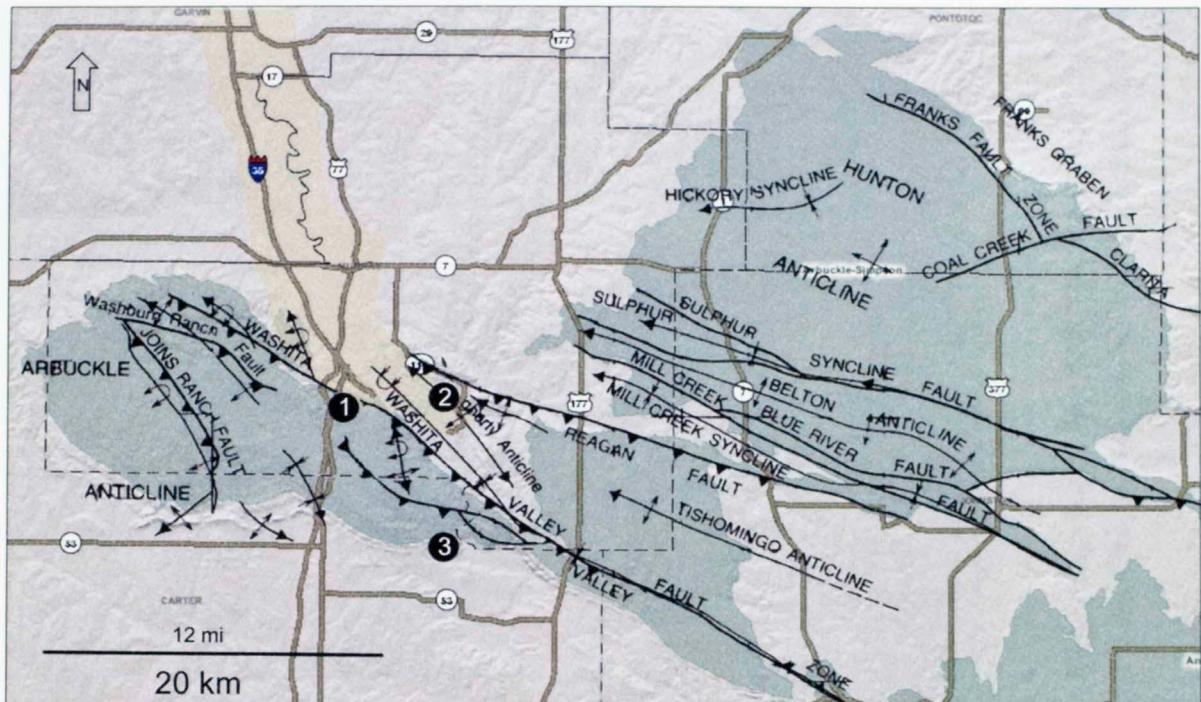


Figure 5 Arbuckle Mountains outline with major faults and folds. Study locations: 1) Oklahoma Highway 77D road cut 2) Vines Creek 3) Cool Creek; modified from Ham (1969).

This study is located in the Arbuckle Mountains of south-central Oklahoma. Woodford Shale outcrops exist in many locations throughout the area; however, exposures of a complete section are rare. The main location for this thesis is Vines Creek ($34^{\circ} 25' 49.836''$ N, $97^{\circ} 4' 32.448''$ W) near the Dougherty Anticline (Figure 5). Other outcrop locations in the Arbuckle Mountains that were also investigated for fracture patterns include a road cut along Oklahoma highway 77D ($34^{\circ} 26' 39.120''$ N, $97^{\circ} 7' 42.996''$ W), and along Cool Creek on the Lazy S Ranch ($34^{\circ} 20' 0.960''$ N, $97^{\circ} 3' 14.040''$ W).

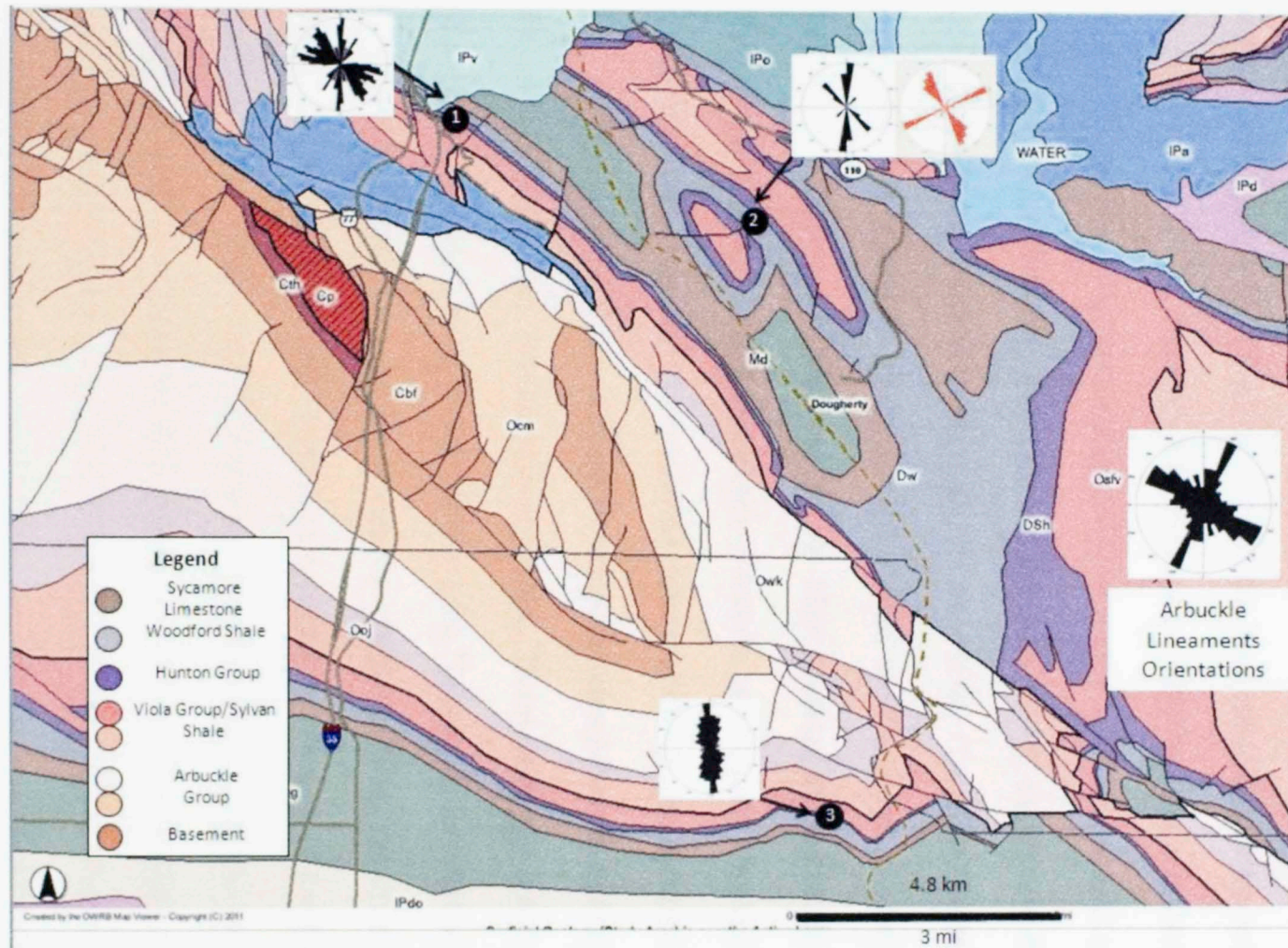


Figure 6 Geologic map of the study area. Outcrop locations: 1) Oklahoma Highway 77D 2) Vines Creek 3) Cool Creek. Measured orientations shown on rose diagrams (modified from Oklahoma Water Resources Board map viewer, 2011)

1.3.1 Structural overview of the Arbuckle Mountains

The Arbuckle Mountains, located north of the Ardmore Basin, consist of northwest-trending anticlines and synclines, separated by northwest-striking faults (Figure 5). The Arbuckle Mountains consist of faulted and folded Precambrian and Paleozoic rocks covered on the west, north, and east by Pennsylvanian and Permian strata and on the south by southward-dipping Lower Cretaceous sedimentary rocks (Ham, 1969). The Arbuckle Mountains, along with the surrounding structural features, are the result of extensive faulting and folding that occurred in Late Mississippian through Late Pennsylvanian time. The compressional forces, which were transmitted from the south south, resulted in the various deformation structures observed today.

Major structures located within the Arbuckles province consist of the Arbuckle, Tishomingo, and Hunton anticlines. These features are the result of faulting and folding that took place in the Late Paleozoic. Located within the Arbuckle Mountains are numerous dip-slip faults including the Washita Valley Fault and the Reagan Fault. The faults represent remnants of the Cambrian Southern Oklahoma Aulocogen and were reactivated during the Arbuckle Orogeny. Most of the smaller structures in the study area are tight concentric folds resulting from the interaction of these two major faults. The study locations are all on the Arbuckle and Tishomingo anticlines in the eastern Arbuckle Mountains (Figure 6). The current regional maximum principal stress orientation (σ_1) is roughly northeast-southwest (Figure 7). This was obtained from the

World Stress Map and the data was originated from analysis of borehole breakouts (Heidback et al. 2008).

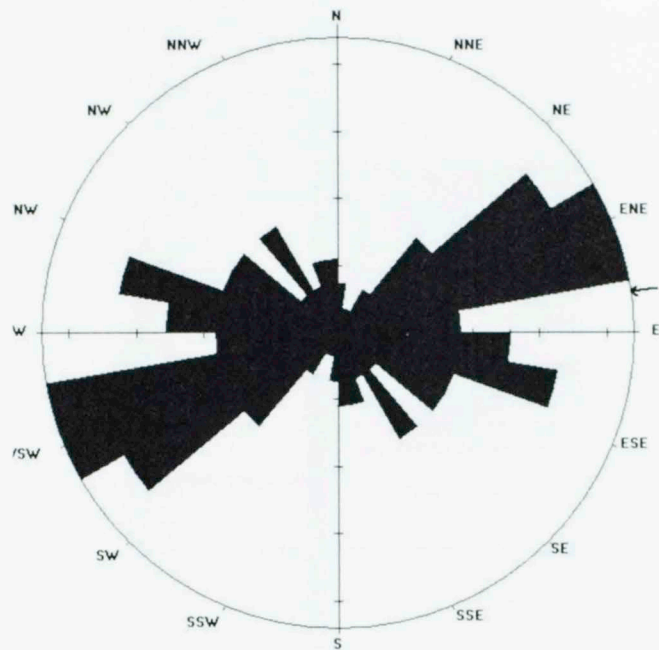


Figure 7 Maximum principal stress orientation northeast-southwest derived from borehole breakouts from Heidback et al. (2008).

1.3.2 Stratigraphic overview of the study area

Series/System		Arbuckle Mountains
Mississippian	Meramecian	Caney Shale
	Osagean	Sycamore Limestone
	Kinderhookian	
Devonian	Famennian	Woodford Shale
	Middle	Hutton Group
	Early	
Silurian	Late	Prisco Formation
	Early	Haragan-Bols d'Arc Fm
		Henryhouse Formation
Ordovician	Late	Clanta Formation
		Cochrane Formation
	Middle	Keel Formation
		Sylvan Shale
Early	Viola Group	
	Simpson Group	
		Arbuckle Group

Figure 8 Stratigraphy for the Paleozoic section in the study area; modified from Ham et al. (1964).

The stratigraphy in the study area ranges from Precambrian granites found in the Tishomingo Uplift to the Pennsylvanian Vanoss Conglomerate (Ham et al. 1964). However, in the outcrops used for this thesis, the stratigraphy typically consists of the Late Ordovician Viola Group to the Mississippian Caney Shale (Figure 8).

The deposition of Paleozoic sediments in southern Oklahoma took place along the Southern Oklahoma Aulocogen. This feature created the accommodation space and tectonic setting which enabled a predominantly marine depositional environment.

Basement

The basement rocks within the Arbuckle Mountains consist of the Cambrian Colbert Rhyolite. This unit is an extrusive igneous flow seen only in the core of the Arbuckle Anticline. The Precambrian Tishomingo and Troy granites constitute the main basement rocks in the Tishomingo Uplift. The basement units are overlain by the Cambrian Reagan Sandstone.

Arbuckle Group (Cambrian-Ordovician)

The Arbuckle Group is the oldest rock seen at the surface and in the wells in the Dougherty area. The Arbuckle Group consists of shallow water carbonates (Ham, 1969). The extreme thickness of the Arbuckle Group, resulted from sedimentation rates equal to the subsidence rate in the aulocogen during Late Cambrian and Early Ordovician deposition (Fay, 1989). The surface expression of the Arbuckle Group is in the form of gray "tombstones" and gently rolling hills supporting few trees.

Simpson Group (Middle Ordovician)

The Simpson Group consists of five formations (from oldest to youngest): Joins, Oil Creek, McLish, Tulip Creek, and Bromide. The Simpson Group sediments were deposited under nearshore conditions and contain more terrigenous clastic strata than do the Arbuckle Rocks. Throughout deposition of the Simpson Group, the Southern Oklahoma Aulocogen subsidence rate equaled the rate of sedimentation.

The Joins Formation consists of thin-bedded limestone and skeletal packstone (Ham, 1969; Fay, 1989). The Oil Creek Formation is composed of a basal clean

sandstone overlain by limestones and shales. The McLish resembles the Oil Creek Formation. Both formations contain basal sandstones; however, the McLish contains more limestone. The Bromide overlies the Tulip Creek. The two have been grouped together for simplification. The Tulip Creek is composed of a basal sandstone, a middle greenish-gray shale, and upper thin-bedded limestones. The Bromide Formation is composed of dense limestone overlying shale and interbedded limestone.

Viola Group (Upper Ordovician)

The Viola Group rests unconformably on the Bromide Formation of the Simpson Group. The Viola consists of three distinct lithologic units: basal carbonate, an intermediate mixed carbonate sequence, and an upper grainstone. The surface expression of the Viola Group is similar to the Arbuckle Group. In the study areas of Vines and Cool Creeks the Viola also forms gently rolling hills with abundant cacti and tall grass. Following deposition of the Simpson Group, the aulocogen began to rapidly subside, which resulted in the upper and middle parts of the Viola being deposited in relatively deep water.

Sylvan Shale (Upper Ordovician)

The Sylvan Shale unconformably overlies the Viola Group. By Late Ordovician time, the deep-water conditions were replaced by shallow-water shelf environments. In outcrop, the Sylvan is a greenish-gray, fissile shale. This shale easily weathers, leading to densely wooded areas.

Hunton Group (Upper Ordovician – Lower Devonian)

The Hunton Group rests unconformably on the Sylvan Shale and contains the youngest rocks of the Early Paleozoic carbonate sequence. The Hunton Group is divided further into (in ascending order): Chimneyhill Subgroup, Henryhouse Formation, Haragan Formation, and Bois d'Arc Limestone (Fay, 1989). These rocks are mainly fossiliferous limestones as well as calcarenites. The limestones in the Hunton mark the end of the carbonate dominated phase of deposition in southern Oklahoma (Ham 1969). The many unconformities within the Hunton Group suggest that the environment of deposition was shallow water in which the sea-level fluctuated numerous times, allowing for sub-areal exposures (Ham 1969).

Woodford Shale (Upper Devonian- Lower Mississippian)

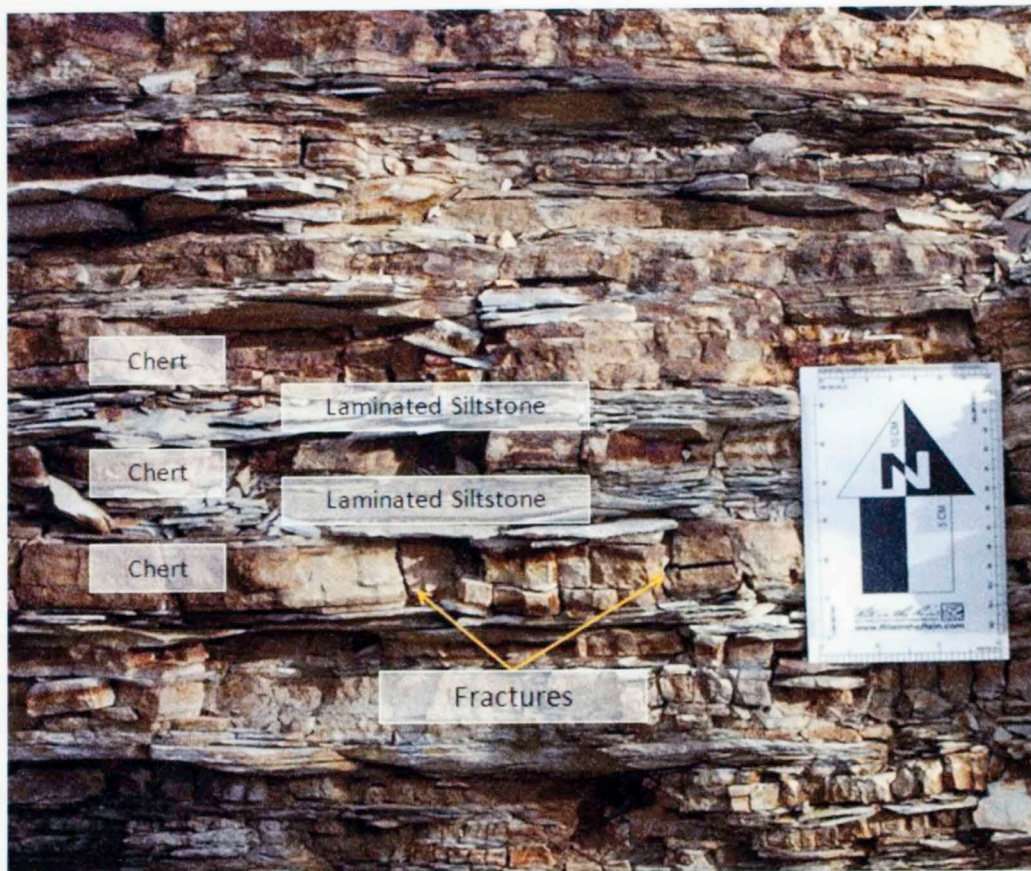


Figure 9 Woodford Shale outcrop with interbedded chert and laminated siltstone.

The Woodford Shale is separated from the underlying Hunton Group by a major unconformity and erosional surface. This sequence boundary marks the beginning of a major marine transgression known as the Kaskasian. Woodford deposition began in Late Devonian Givetian stage, approximately 392 mya, and lasted until the Kinderhookian stage of the Early Mississippian, approximately 359 mya (Over and Barrick, 1990; Over, 1992). The Woodford Shale was deposited in a marine, oxygen-poor environment and the internal stratigraphy is dominated by thinly laminated shales (Figure 9), interbedded chert, calcareous laminae, and phosphatic concretions (Cardott and Lambert, 1985; Sullivan,

1985; Lambert, 1993). The Woodford is typically subdivided into lower, middle and upper members (Cardott, 2005). Members divisions are based on geological, paleontological, geochemical and electrical log variations (Sullivan, 1985; Hester et al., 1990; Lambert, 1993; Cardott, 2005). The total thickness in the study area is approximately 75 meters (Krystyniak, 2006).

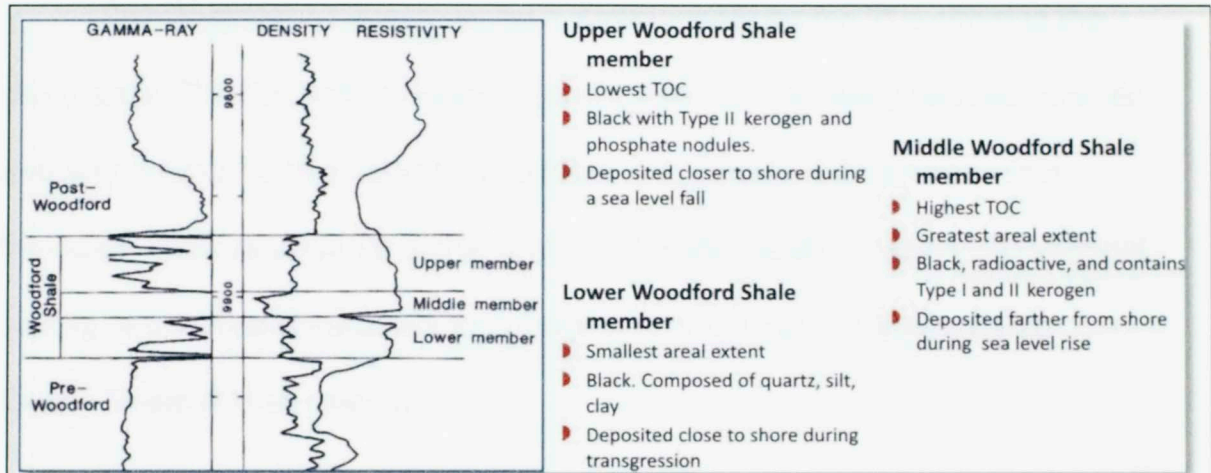


Figure 10 Woodford Shale members as described in electric logs, lithofacies, depositional environment (modified from Cardott, 2007 and Slatt et al., 2011)

Alternating sequences of laminated shales are rich in organic matter.

Total organic carbon (TOC) varies with location and distribution within the stratigraphic section; however, values of 10% TOC or greater are common. The kerogen type is also variable, but the Woodford Shale contains mostly Type II kerogen (Cardott, 2005). In the study area, the maturity (R_o) is approximately 0.70 (Cardott, 2005) indicating peak maturity stage of hydrocarbon generation (Figure 10).

The Misener Sandstone marks the base of the Woodford Shale, but this unit is absent at the study locations. The Woodford is recognized on logs by a sharp increase in gamma-ray greater than 200 API units. This increase is

common to many Devonian shale formations in the United States (Over, 1992). The middle-upper Woodford boundary is marked by a very high gamma-ray signature, and coincides with the Devonian-Mississippian boundary (Cardott, 2005).

Sycamore Limestone (Mississippian)

The Sycamore Limestone rests conformably on the Woodford in the study area. The Sycamore is made up of cycles of massively bedded, micritic and silty limestone beds and thin-bedded, calcareous, dark shales. This formation likely represents a change from the siliciclastic, marine depositional setting of the Woodford Shale to a more carbonate-rich, marine setting.

Caney Shale (Mississippian)

The Caney Shale is the last major, organic-rich condensed section in the study area. The sequence is characterized by highly fissile, marine shales and carbonate concretions.

1.4 Fractures

Natural fractures exist as the three fracture modes (Figure 11). Under mode I, the two blocks move normal to the fracture surface and results in tensile fractures or joints. Under mode II and III the blocks slip parallel to the fracture surface forming a fault. Mode I is of particular interest in this study because it often results in creation of void space and can act as conduits for fluids in the subsurface (Nelson, 1985).

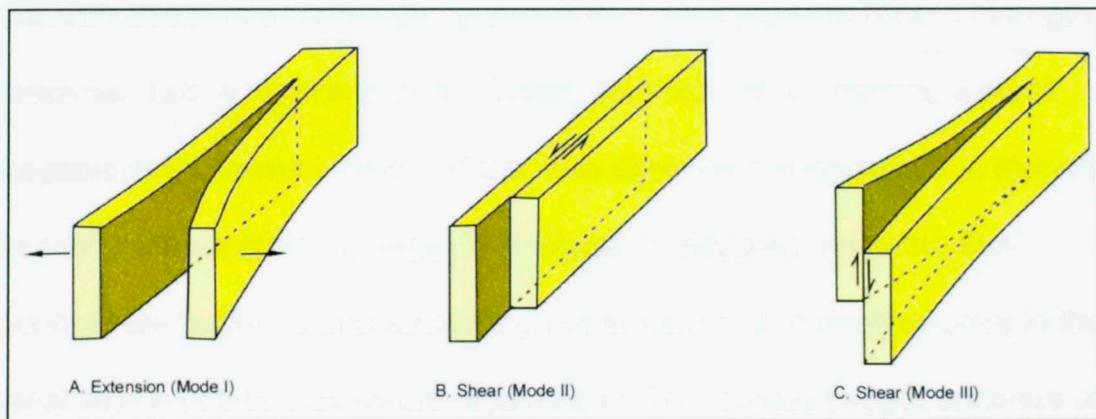


Figure 11 Fracturing modes: Mode I extension, Mode II sliding, Mode III tearing (Ataman, 2008).

1.4.1 Failure

Brittle failure in solids begins with stress amplification around a critical flaw (e.g., Griffith, 1921; Pollard and Aydin, 1988). A flaw in the material might be any deviation from homogeneity, whether in the form of a weak grain boundary, a contact between layers, or a newly formed void space, to name a few. In quasi-static tensile fracturing, the stress applied to the material is initially stored as elastic energy. The stress magnifies and the critical flaw forms an ellipse with stress tips. When the local stress moves past the tensile strength of the material, failure begins to occur. When the initial failure occurs, a crack propagates and creates a new surface. The stresses are relieved and there is a decrease in stored elastic energy. The failure propagates along the flaw, creating newer surfaces and advancing the stress front to another point in the material where elastic energy can again build. This process might continue until the fracture reaches an interface where the stress is redistributed or a fluid enters the void space created by the failure and precipitates enough minerals to "heal" the fracture. Rock strengthening by mineralization can arrest fractures temporarily by creating a "vein", or mineral-filled fracture, until sufficient stresses build up to overcome this effect. However, the mineralized surface is often a weak surface due to poor bonding between the host materials and the vein fill and can thus create a flawed surface prone to re-fracture.

Shear failure occurs by coalescence of micro flaws that form a weakness zone (Reches and Lockner, 1994). As remote stresses increase, they begin to reach the failure envelope of the material, the small micro cracks coalesce and

being to align until a slip surface is formed. The deformation is then accommodated along the newly formed fault plane, which fails by modes II and III. Since the deformation is accommodated in three dimensions, four sets of shear fractures form (Reches, 1983).

1.4.2 Principal Stresses

It is generally accepted that fractures grow perpendicular to the least compressive principal stress (σ_3) and parallel to the maximum compressive principal stress (σ_1). Therefore the opening of tensile fractures occurs in the direction of σ_3 . The opening front or fracture tip, represents the amplified stress area of the growing crack. A change in the state of stress or a relaxation in the stresses can affect propagation direction (Engelder, 1987). Contrasts in tensile strength at layer boundaries can also redistribute the stresses to cause a crack to change its propagation direction or to stop propagating. A growing fracture creates a "stress shadow" around it due to stress relaxation and thus inhibiting the growth of additional fractures directly adjacent to it. Fractures that occur in close proximity can cause a local stress field that may counter the mechanism mentioned above. In close proximity, an opening joint may lead adjacent cracks to seal from localized compression (Germanovich and Dyskin, 2000).

1.4.3 Layers

Fractures are inherently complex. A fracture face is described as having a point of origin or a nucleation point which leads to the subsequent propagation (Engelder, 1987). The presence of layers in sedimentary rocks creates a complex exchange between material heterogeneity and mechanical anisotropy which result in a variety of dynamic changes which range from the starting point of a crack to the length and shape of fractures. Understanding the interaction among layering, stratigraphy and fractures is the primary aim of this study.

The Woodford Shale is a laminated or layered, organic-rich shale with two distinct mechanical properties. Some layers can be defined as mechanically brittle, while others tend to be mechanically ductile. This material property has a fractal property that can be noted from the microscopic to the reservoir scales (Slatt et al., 2010). The brittle layers in the Woodford are beds rich in quartz (mostly as radiolarian chert) and calcite that typically fail by jointing. The joints in these brittle layers are predominantly perpendicular to the bedding surfaces. The ductile layers are rich in clay minerals and have high organic carbon content. Ductile materials can deform plastically and fail by shear under rapid or high stresses (Cox, 1951).

2. ANALOG MODELING

Analog experiments are used by structural geologists to approximate the behavior of rocks in the field, with the goal of gaining a better understanding for natural deformation processes. These experiments are done with analog materials that broadly represent the mechanical properties of rocks. The process is not a scale modeling experiment, yet the results can be used to further understand the dynamics of deformation and failure.

2.1 Methods

Clay extension experiments were conducted in the Physical Modeling Laboratory (PML) at the University of Oklahoma (OU), which is part of the laboratory of Dr. Shankar Mitra, School of Geology and Geophysics.

The experiments were conducted with wet clay and Play-Doh to observe the deformation in sedimentary rock layers. The clay, with density of about 1.6 g/cm^3 , behaves like a brittle solid and fails by fracturing under tension under experimental stresses. The clay is assumed to be an analog for the brittle layers (e.i. chert) of the Woodford Shale. Play-Doh is a combination of mostly flour and water, has a density of 1.25 g/cm^3 , and behaves like a plastic material under tensile stress. It is assumed to be an analog for the ductile layers of the Woodford Shale.

The apparatus consists of a large metal table with a fixed Plexiglas wall on one side, and a movable Plexiglas wall on the other (Figure 12). The movable Plexiglas wall is connected via gears to an electronic control board

that regulates the rate of movement. The table can be operated in compression or extension modes. Only extension was used for these experiments.

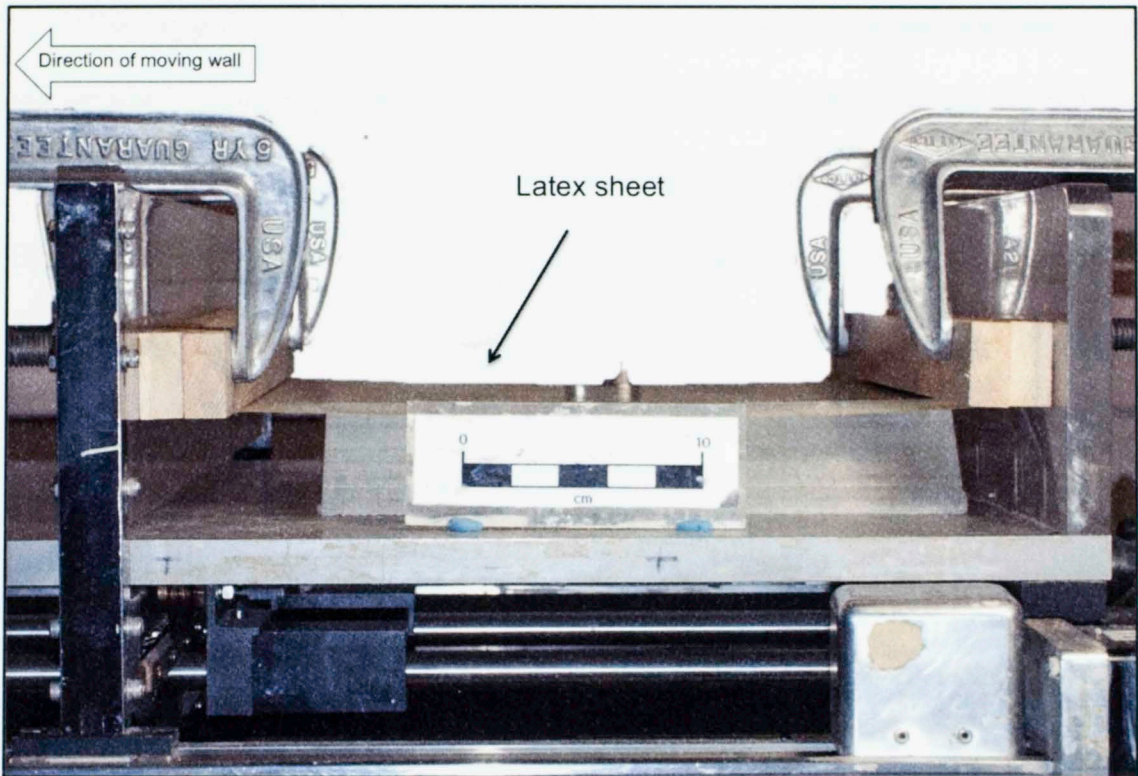


Figure 12 Apparatus used for analog modeling experiments. The clay and Play-Doh models were mounted on the latex sheet.

The analog materials were mounted directly on a large sheet of latex. The latex sheet was attached with C clamps to the Plexiglas walls of the table. The sheet was carefully mounted so it was slightly stretched directly above an aluminum metal block placed on the table.

The boundary conditions for all the experiments were the same. The models were deformed by pulling a latex layer from one side (left), while fixed at the other side (right). The clay and Play-Doh models were mounted on a thin latex sheet to generate uniform stretching. The latex sheet was pulled at a constant rate and the material stretched and increased in length but retained the same volume. At the base, the wet clay or the Play-Doh were 'glued' to the latex

sheet by their self-adhesion, and the latex extension was uniformly transferred to the model above.

The upper surface of the model was free to deform upward and the sides were allowed to deform sideways. When a layer of Play-Doh was at the bottom of the model in direct contact with the latex sheet, the material underwent thinning with extension. This thinning allowed for a minor downward movement of the clay above it. The Play-Doh also behaved like the latex sheet, and transferred the stretching uniformly to the clay layer.

As shown in Table 1 four model setups were tested: 1. Play-Doh 2. Play-Doh/clay 3. Play-Doh/clay/Play-Doh 4. Clay/Play-Doh/clay.

Analog Experiment Parameters			
Setup	Materials	Rate	Duration
1	Play-Doh	0.381 cm/min	30 minutes
2	Play-Doh/clay	0.381 cm/min	25 minutes
3	Play-Doh/clay/Play-Doh	0.381 cm/min	35 minutes
4	clay/Play-Doh/clay	0.381 cm/min	30 minutes

Table 1 Setup of the analog models.

Setup 1

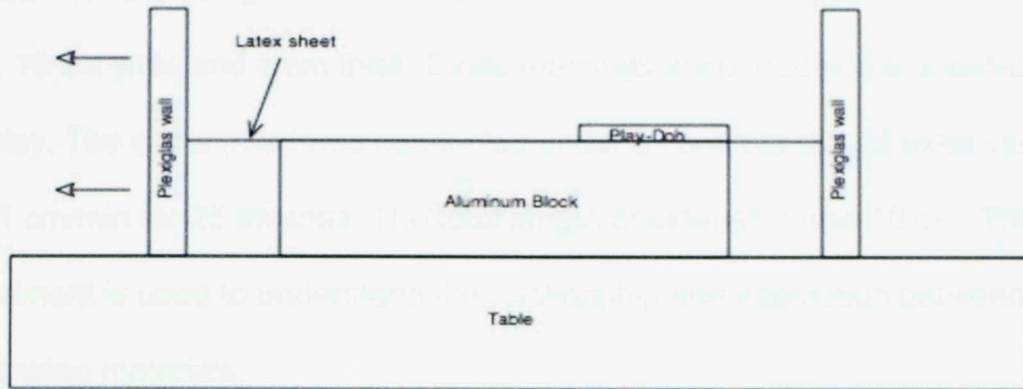


Figure 13 Setup for experiment 1: Play-Doh extensional (not to scale).

The first experiment was setup using a single sheet of Play-Doh (Figure 13), which was 12cm long, 12 cm wide and 1 cm thick. The experiment was conducted under a constant rate of latex extension of 0.381cm/min for 30 minutes. This experiment was used to test the new analog material for ductile rocks.

Setup 2

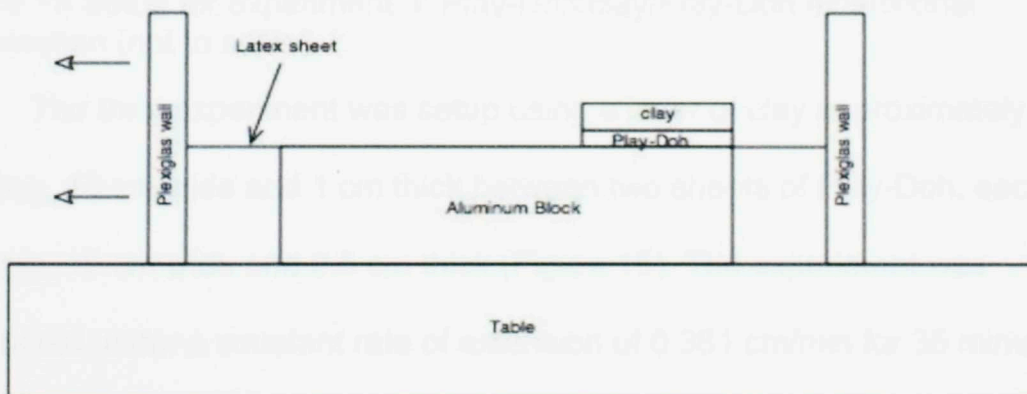


Figure 14 Setup for experiment 2: Play-Doh/clay extensional deformation (not to scale).

The second experiment was setup using a single layer of Play-Doh (Figure 14) 12cm long, 10 cm wide and 0.5 cm thick and a layer of clay 12 cm long, 10 cm wide and 1 cm thick. Circle markings were made on the surface of the clay. The experiment was conducted under a constant rate of extension of 0.381 cm/min for 25 minutes. The total length of extension was 10 cm. This experiment is used to understand the relationship and interaction between the two analog materials.

Setup 3

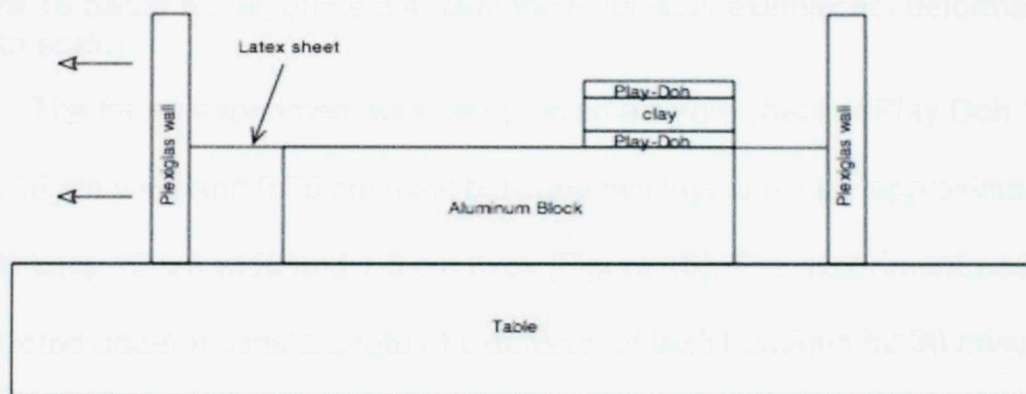


Figure 15 Setup for experiment 3: Play-Doh/clay/Play-Doh extensional deformation (not to scale).

The third experiment was setup using a layer of clay approximately 12 cm long, 10 cm wide and 1 cm thick between two sheets of Play-Doh, each 12 cm long, 10 cm wide and 0.5 cm thick (Figure 15). The experiment was conducted under a constant rate of extension of 0.381 cm/min for 35 minutes. The total length of extension was 13.7 cm. This setup tested a brittle-ductile sequence.

Setup 4

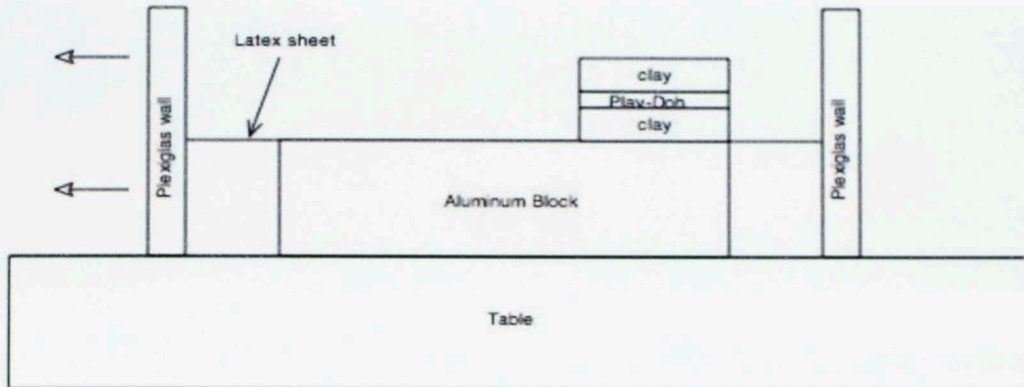


Figure 16 Setup for experiment 4: clay/Play-Doh/clay extensional deformation (not to scale).

The fourth experiment was setup using a single sheet of Play-Doh 12 cm long, 10 cm wide and 0.75 cm thick between two layers of clay approximately 12 cm long, 12 cm wide and 1.6 cm thick (Figure 16). The experiment was conducted under a constant rate of extension of 0.381 cm/min for 30 minutes. The total length of extension was 11.4 cm. This setup also tested a brittle-ductile couplet with more over-burden.

2.2 Results

Setup 1

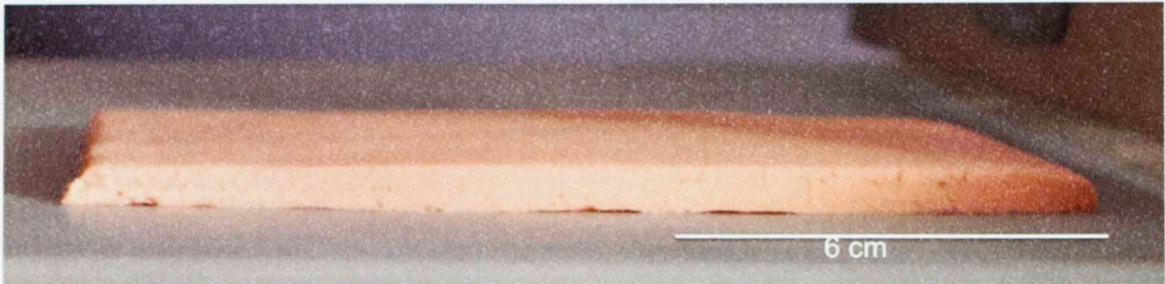


Figure 17 Setup 1 showing a single sheet of ductile Play-Doh after extension.

A thin layer of Play-Doh was extended at a constant rate for 30 minutes. The layer deformed but did not fail, and it underwent thinning (Figure 17) from an initial thickness of 1 cm to a final thickness of 0.75 cm.

Setup 2

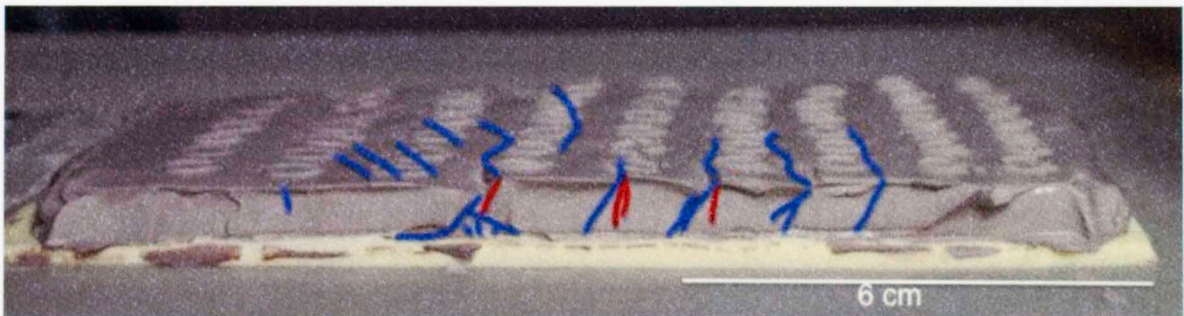


Figure 18 Setup 2 showing a ductile Play-Doh layer (bottom) and a brittle clay layer (top) after extension. Early stage tensile fractures (red). Inclined shear fractures (blue) seen on the side and top of the clay.

The Play-Doh was the first layer, which remained 'glued' to the latex sheet during the complete run of the experiment. Additionally the Play-Doh underwent thinning as in Setup 1. The clay layer above the Play-Doh began to fail as small tensile fractures (Figure 18) nucleated from the tips of the circle markings on the clay surface. The segments began to propagate at their tips towards the sides of the model. With increasing extension, the segments began

to coalesce and form semi-planar shear fractures (Figure 19) with slip in the direction of extension. These fractures could be classified as normal faults. At the late stages of the experiment, the normal faults increased in displacement and slickenlines were observed on the fault scarps. Also, two sets of shear fractures formed at an angle to the first faults (Figure 19). The late stage shear fractures are strike-slip faults and displacement was observed.

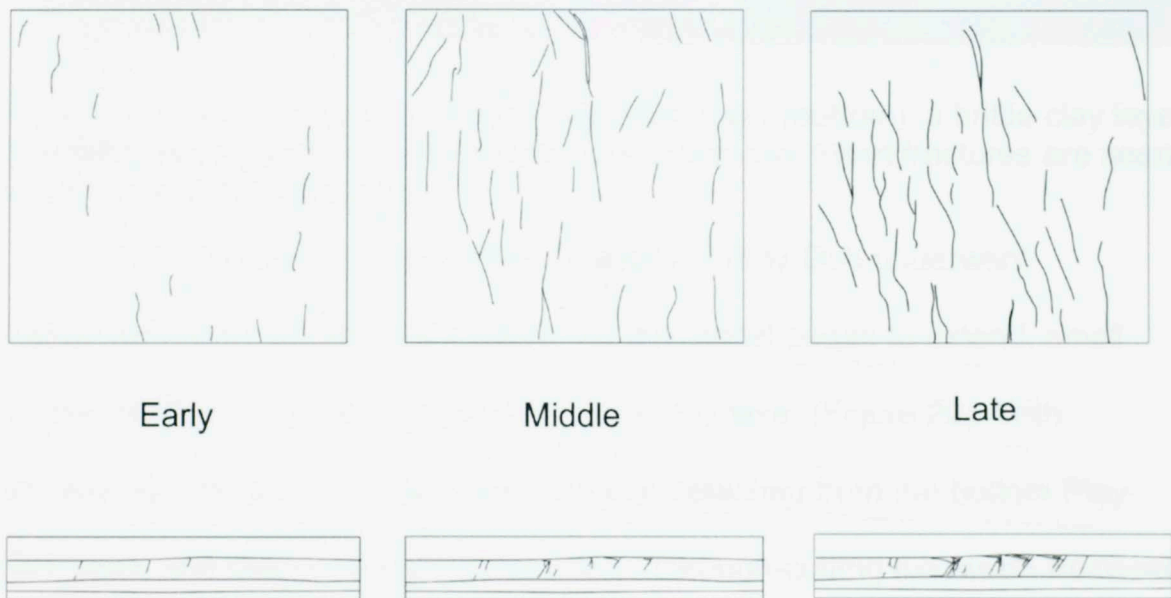


Figure 19 Top and side view of Setup 2 showing progression of fracturing in the early, middle and late stage of the experiment.

The side view revealed the initial tensile fractures as they formed from the top edge, and propagated downward. With increasing extension the fractures began to rotate and slip occurred along the fault planes in the direction of extension. In the late stage of the experiment a new set of shear fractures formed on the surface with slip at an angle to the direction of extension (Figure 19).

Setup 3

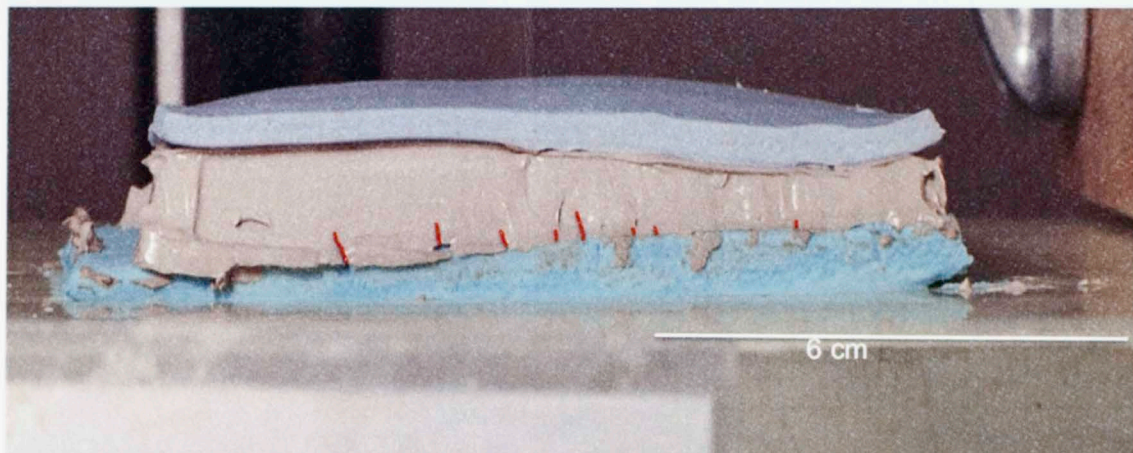


Figure 20 Setup 3 showing a ductile Play-Doh layer (bottom), a brittle clay layer (middle), and a ductile Play-Doh (top) after extension. Short fractures are seen on the side of the clay layer.

The clay layer between two thin layers of Play-Doh underwent deformation without significant failure. As the model began to extend, small tensile fractures nucleate at the base of the clay layer (Figure 20). With increasing extension, the clay layer became detached from the bottom Play-Doh layer and slipped along the boundary. Through-cutting extension fractures did not occur in the middle clay layer. In the late stage of the experiment, all of the deformation was accommodated in the basal Play-Doh layer, while the clay and upper Play-Doh layers did not deform further.

Setup 4

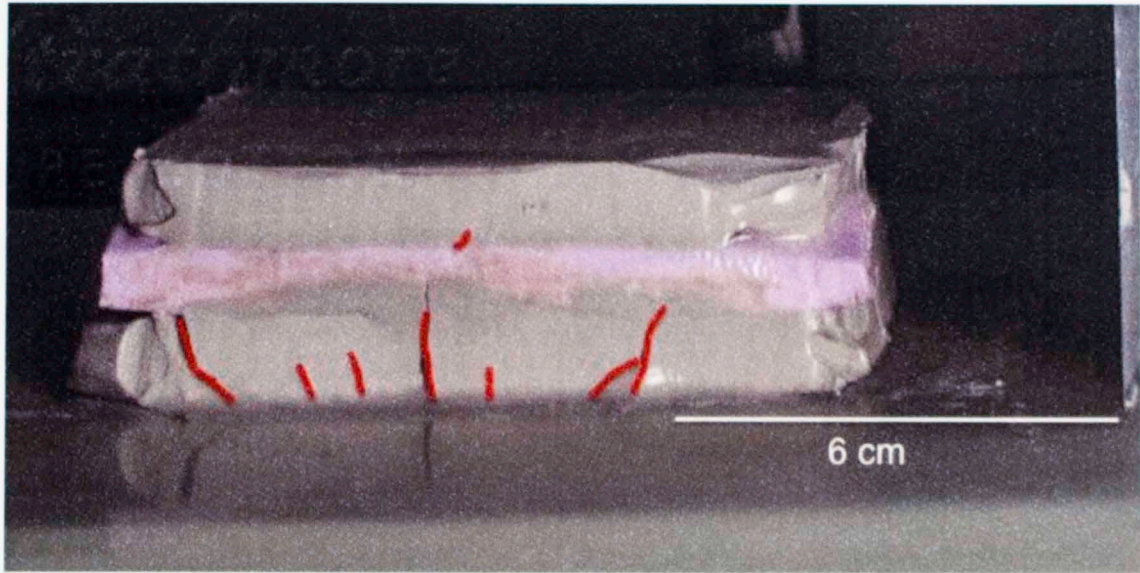


Figure 21 Setup 4 showing a brittle clay layer (bottom), a ductile Play-Doh layer (middle), and a brittle clay layer (top) after extension. Fractures are seen on the side of the clay layers.

The Play-Doh layer between two layers of clay deformed but did not fracture under extension. Multiple tensile fractures formed in the bottom clay layer (Figure 21). The fractures started to form at the clay/latex boundary and propagated upward. The fractures stopped propagating when they reached the Play-Doh layer. In the late stage of the experiment, a small tensile fracture had begun to nucleate in the upper clay layer. The late stage fracture originated at the clay/Play-Doh boundary.

A top view for this experiment was not available, and visual inspection of the free clay surface at the top of the model did not reveal surface cracks. Also, model preparation created clay smears on the Play-Doh surface leading to apparent tensile fracturing in the Play-Doh. This is a defect of the preparation and was disregarded.

2.3 Discussion

The clay/Play-Doh experiments are assumed to be analogs for the stratigraphic relationship of the two principal mechanical layers described from outcrop. The brittle-ductile couplet was modeled with two analog setups: clay-Play-Doh-clay (brittle-ductile-brittle) and a Play-Doh- clay-Play-Doh (ductile-brittle-ductile). The first setup was most effective at modeling the observed outcrop stratabound fracture type.

The clay-Play-Doh-clay model in Setup 4 (Figure 21) also included the latex sheet as an additional ductile layer. In this experiment, fractures propagated from the base of the first clay layer and remained perpendicular to the layers. Fractures stopped propagating when they reached the middle ductile layer. Near the end of the experiment run, a small fracture had propagated on the second clay layer but never reached the surface of the clay.

Setup 3 (Figure 20), which had a sequence of Play-Doh- clay-Play-Doh, showed early stage formation of tensile fractures. These small cracks formed at the base of the middle clay layer. However, because the layers were not completely bonded together, much of the extension was accommodated by shearing along the ductile-brittle boundary and was not transferred to the brittle layer.

Although the 3rd setup was unsuccessful at modeling tensile fractures in the brittle layer, the experiment did present an interesting result. The propagation of tensile fractures occurred at the mechanical boundary, which

was in accordance with the proposed mechanism for tensile-fracture propagation in layered, anisotropic materials (Gross, 1993; Bahat et al., 2005). Furthermore, the model predicts the formation of layer-parallel fractures in layered sequences which may not be strongly attached or bonded. This type of deformation may predominate over tensile fracturing in poorly compacted sediments.

Setup 2 (Figure 18) was also significant in explaining the mechanisms for the formation of shear fractures in a brittle-ductile material. During the early stages of the experiment, small tensile fractures began to form at the surface. Extension during late-stage deformation resulted in block rotation and slip along the fracture plane (Figure 19). The model also upholds the mechanism that larger faults form by small segments coalescing together to form a long, continuous fault zone. The zigzag pattern of the faults is due to the three dimensionality of faulting as predicted by Reches (1983) and Sagy et al., (2003).

3. FIELD WORK

3.1 Methods

Three outcrop locations were used for this study. Along Oklahoma Highway 77D the Woodford Shale is exposed as overturned beds on the north limb of the Arbuckle Anticline. The Vines Creek outcrop is located near the Dougherty Anticline and consists of tilted beds. The Cool Creek Woodford section is located on the south limb of the Arbuckle Anticline and it includes several isolated exposures of vertical beds (Figure 6).

In the field, the stratigraphic sequence was measured using a Jacob's Staff with a Brunton compass to account for bed inclination. Gamma ray data was collected in counts-per-second every 60 cm with a hand-held scintillometer for total gamma-ray, potassium, thorium and uranium.

A scintillometer (Figure 22) is a device that is typically used to detect variations of radioactive elements in a given area. This device can also be used like a borehole gamma-ray sonde to create a signature of natural gamma-ray emission from strata for use as a lithology and correlation tool (Slatt et al., 1995).



Figure 6 Scintrex GRS-500 hand-held detector used to create outcrop gamma-ray logs.

The unit used for this study was a Scintrex GRS-500 hand-held detector. Five readings were collected at each point for a count time of three seconds each. Then the arithmetic mean of the five readings was obtained to denote the radioactivity at each point (Slatt et al., 1995). The data from each point was plotted along the length of the outcrop to construct a profile of radioactivity that looks much the same as a gamma-ray log with the exception that the outcrop log measures radioactivity in counts per second (cps). Spectral gamma-ray data was collected and plotted using the same technique.

Due to the instrument's recording diameter (0.3 m), readings obtained from thin beds are susceptible to "noise" from adjacent beds (Slatt et al., 1995). This could not be corrected and was simply ignored.

3.1.1 Outcrop descriptions

The Vines Creek outcrop descriptions included field examinations, photographs and rock samples. Field descriptions were done with a hand lens and visual inspection. Lithofacies were subdivided in terms color, grain size, bedding characteristics and calcareous content. Calcareous layers were identified based on reactivity to weak HCl acid, ranging from very calcareous to mildly to non-calcareous.

3.1.2 Fracture Analysis

Fracture azimuth was measured using a Brunton compass; spacing was determined by visually counting fractures over a distance of approximately 2 meters. Fractures were also classified as open or closed and mineralized fractures were noted. Fracture azimuths were plotted on rosettes for analysis and interpretation. Fracture orientations were also obtained using high-resolution pictures of outcrop taken with a known orientation. The fracture markings were digitized using the software Digicracks developed by Jefferson Chang and Dr. Ze'ev Reches of OU for Matlab and exported x-y locations to a spreadsheet. Basic trigonometric functions were applied to obtain the azimuth of each digitized line. This information was also plotted on rose diagrams. Fracture maps were constructed by digitally tracing fractures on the digital images. Digital images of bedding planes and vertical outcrop sections were used. The fracture maps are displayed in 50cm² survey maps and the density of fractures calculated by point counting them in the survey square. A traditional

scan line method was also digitally applied to determine fracture spacing and to relate to bed thickness.

3.2 Results

3.2.1 Outcrop Lithofacies

Outcrop Lithofacies				
Lithofacies	Color	Grain size	Bedding	Calcareous
Calcareous mudstone	dark grey-black	clay	Sharp, <2 cm thick	very
Laminated siltstone	dark brown-black	silt	Rippled or wavy, fissile, <1 cm thick	non
Chert	dark grey-black	microcrystalline	Sharp, 2-10 cm thick	non
Phosphatic mudstone	dark grey-dark blue	clay	Irregular <2 cm	moderately
Organic-rich claystone	dark grey-black	clay	Rippled and irregular, fissile, <1 cm thick	non

Table 2 Outcrop lithofacies classification from the Woodford Shale outcrops.

Five distinct lithofacies were recognized in the Woodford Shale outcrops examined (Table 2). The first is a calcareous mudstone that is dark grey or black in appearance. Second is a laminated siltstone, which ranges in color from dark brown to black. This lithofacie is also fissile and non-calcareous. The third type is a thickly bedded, microcrystalline chert, which is dark grey or black. The lithofacie is a mudstone that contains abundant phosphatic or calcareous nodules. The color is dark grey or dark blue and the concretions are concentrically layered. The fifth is a non-calcareous, organic-rich claystone, which is dark grey or black and often bituminous (Figure 23).

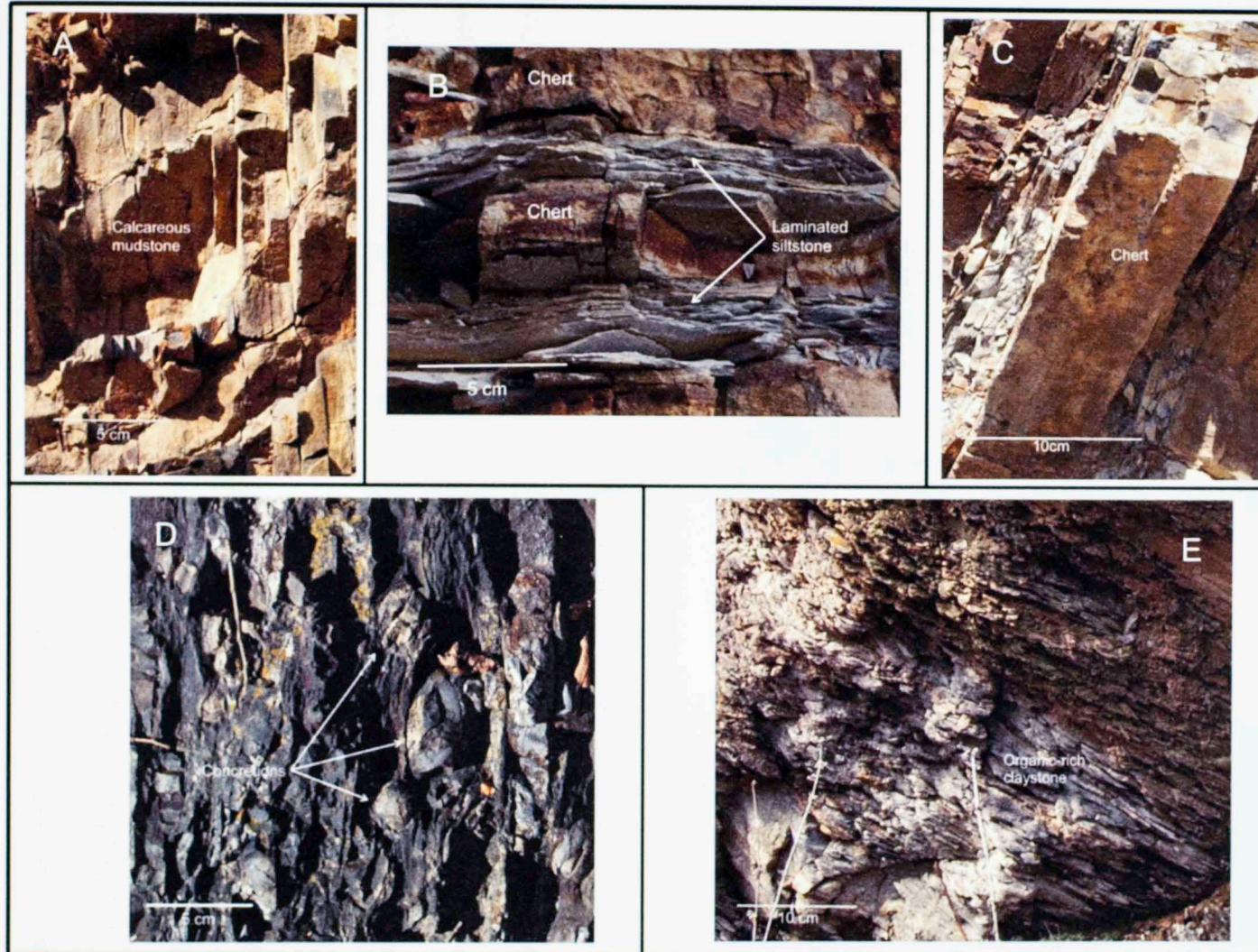


Figure 23 Woodford Shale outcrop lithofacies. A. Calcareous mudstone B. Laminated siltstone C. Chert D. Phosphatic mudstone E. Laminated organic-rich claystone.

3.2.2 Outcrop fracture types

Outcrop Fracture Types			
Fracture	Opening	Length	Host Lithofacies
Strata-bound	Open, perpendicular to bedding	<10 cm	Chert and calcareous mudstone
Layer-cutting, angled	Closed	<10 cm	Organic-rich claystone and Laminated siltstone
Layer-cutting, jagged	Open	Between 10 cm and 1 m	Any
Curved	Open/Mineralized (calcite, gypsum)	<10 cm	Organic-rich claystone
Swarming	Open/Mineralized	Between 1 and 5 m	Any
Faults	Open and closed	Between 10 cm and 5 m	Any

Table 3 Outcrop fracture classification from the Woodford Shale outcrops.

The fractures from all the locations examined were classified into six distinct types (Table 3). The classification is independent of orientation and based solely on shape and interaction between layers (Figure 24). The first fracture type is strata-bound, straight, systematically spaced, and can be open or mineralized. This fracture type forms perpendicular to bedding in chert or calcareous mudstones. The second fracture type is layer-cutting, angled, and nonsystematic in spacing. This fracture type can be open or mineralized and cut across different layers. A third type of fracture is layer-cutting, jagged in shape, and nonsystematic in spacing. This type often forms tensile and small shear fractures, and often cuts across several layers of varying lithology. The fourth fracture type is curved, non-systematically spaced and mineralized. This type of fracture is small and can cut across a few layers, but it is restricted to organic-

rich claystones. The curved shape of the fractures resembles sedimentary structures such as troughs and ripples in the host mudstone. The dominant mineral fill is typically calcite, but gypsum, pyrite and quartz are also common. The fifth fracture type is swarming, typically nonsystematic in spacing, and often occurs across varying lithofacies. This fracture type can be open or closed and typically cuts across many layers. The sixth type of fracture is faults as small shear fractures that can be segmented and intersect many layers. Fault movement on this fracture type can be a combination of Mode II and III shear failure.

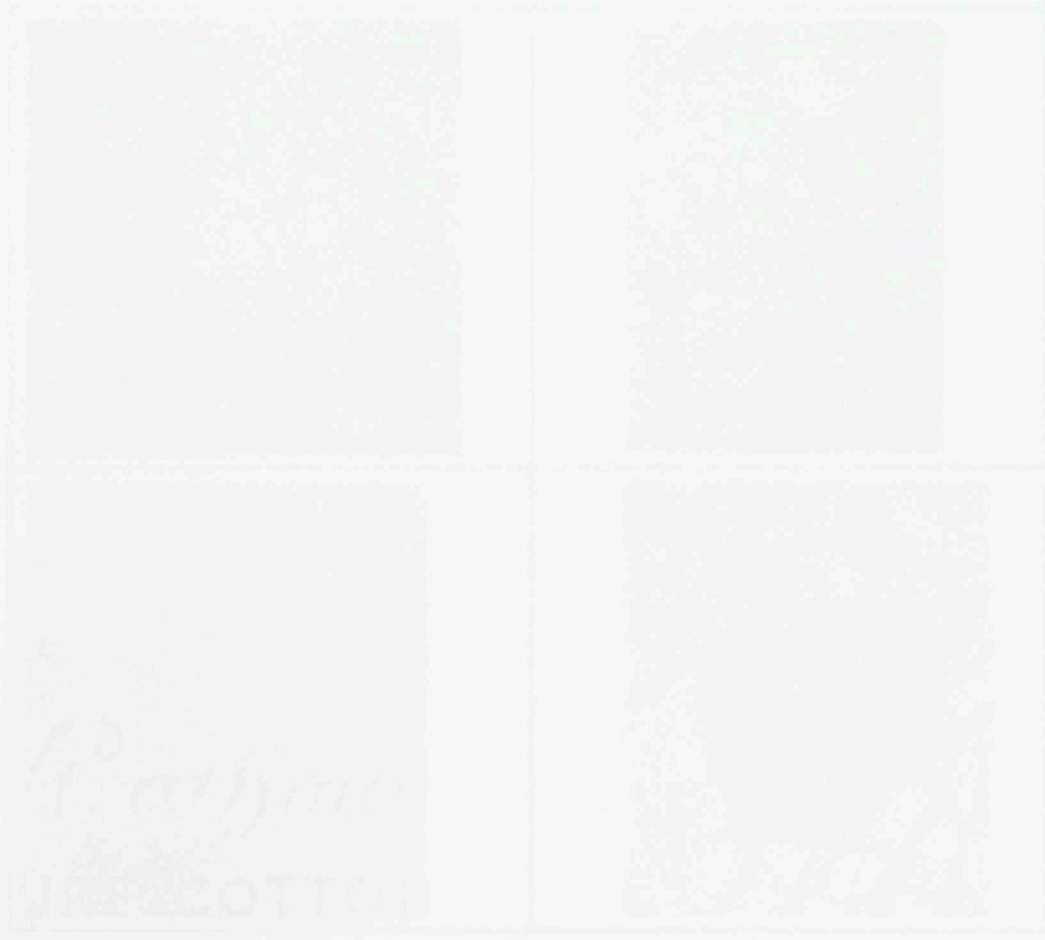


Figure 24 Modified from *Carbonate Reservoirs*. A. Struck-slip B. Layer-parallel C. Faults D. Curved E. Swarming F. Faults. Images A-C were taken perpendicular to the fractures. Images D-F were taken parallel to the orientation of bedding planes.

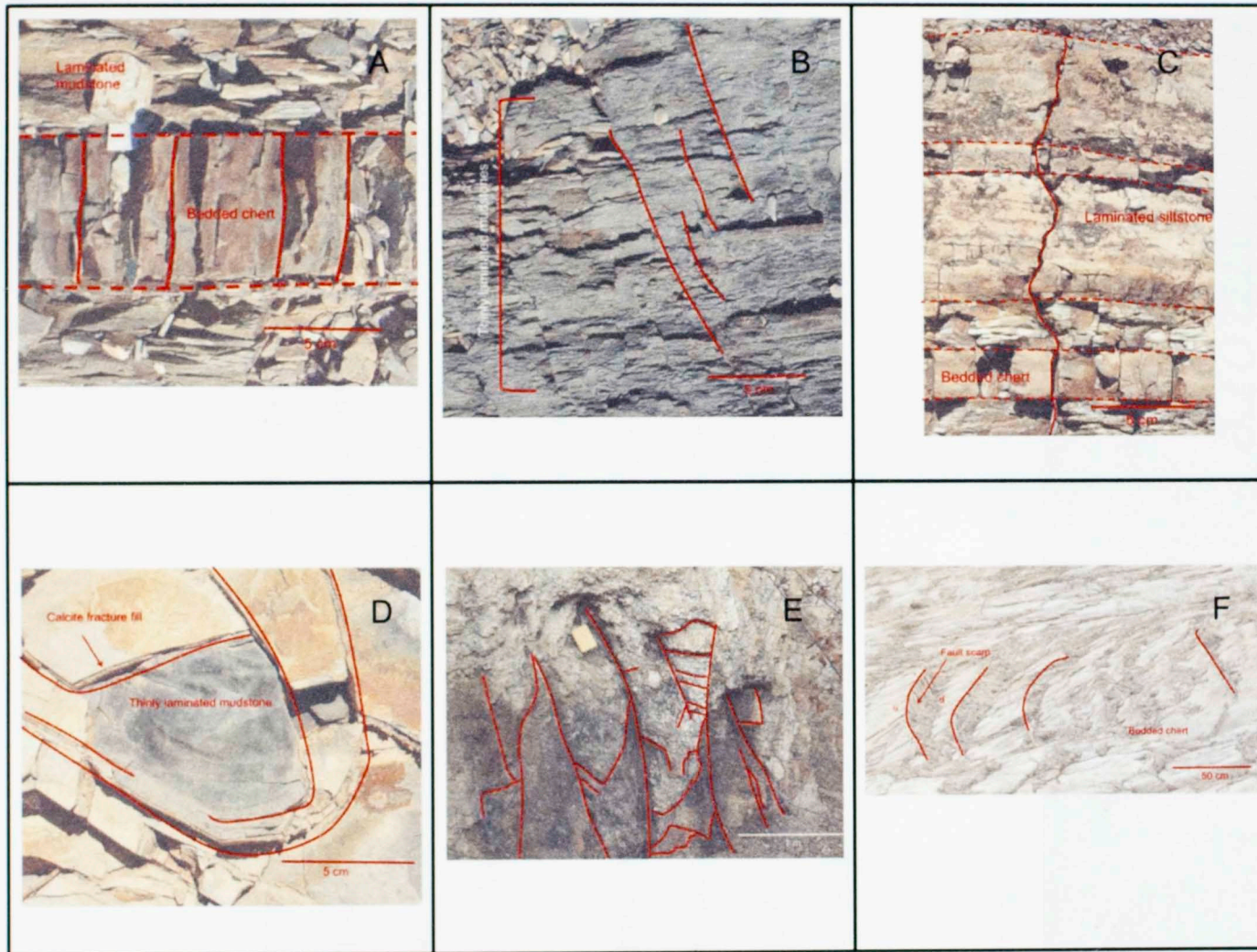


Figure 24 Woodford Shale outcrop fracture types. A. Stratabound B. Layer-cutting angled C. Layer-cutting jagged D. Curved E. Swarming F. Faults. Images A-C were taken perpendicular to the orientation of bedding planes. Images D-F were taken parallel to the orientation of bedding planes.

3.2.3 Vines Creek



Figure 25 Vines Creek Woodford Shale outcrop of north-dipping beds, looking west.

The Vines Creek outcrop (Figure 25) is a continuous exposure of the Woodford Shale along a small stream near the Dougherty Anticline. The stratigraphic sequence was measured at 75 meters, but some areas were covered with soil and vegetation. A small portion of the overlying Sycamore Limestone is present near the axis of the syncline.

At this location all rock and fracture types were present, but the most common fracture types were stratabound and layer-cutting angled. The stratabound fractures are restricted to chert or calcareous mudstone beds. Layer-cutting angled fractures are present in organic-rich claystones and laminated siltstones.

Fracture statistics

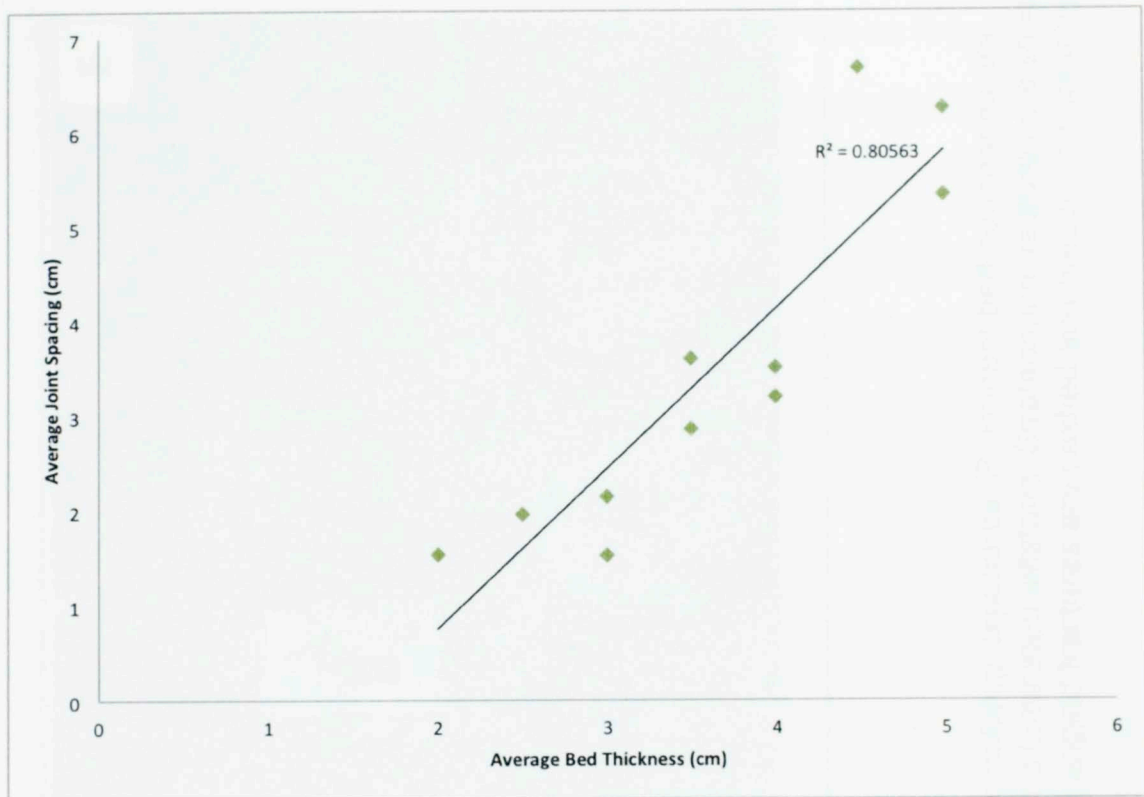


Figure 26 Vines Creek graphical relationship between bed thickness and joint spacing for the stratabound fracture type.

The relationship between spacing and bed thickness (Figure 26) was obtained by measuring an 80-cm scan line digitally with high-resolution images of several outcrop exposures along Vines Creek. The scanlines varied in length from 50 cm to 1 m depending on the quality of the exposure. Bed thickness was not constant, so an average was used. The relationship shows a positive linear trend with good correlation ($R^2 = 0.81$). In thin beds, fractures are more closely spaced, increasing their density.

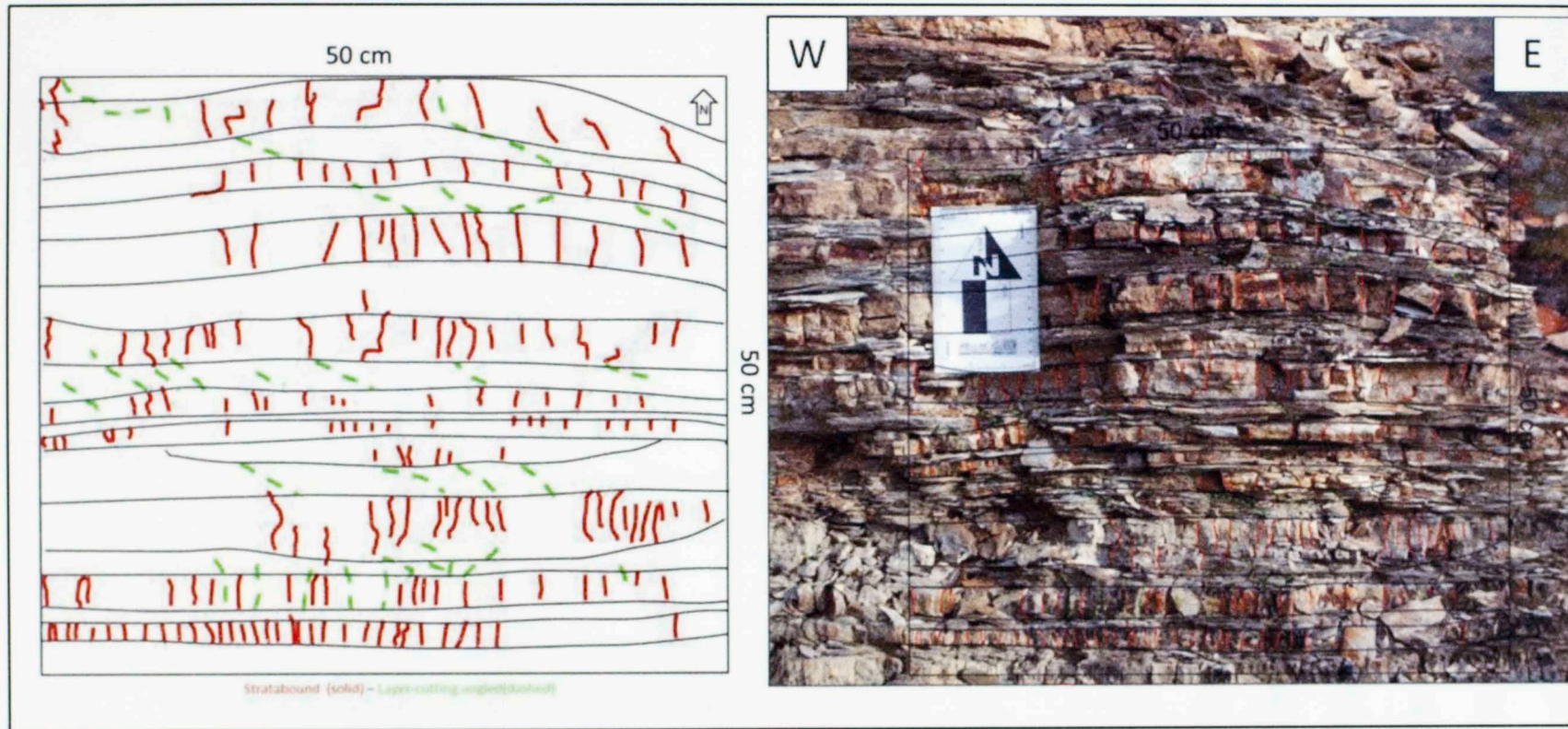


Figure 27 Vines Creek fracture survey square completed from outcrop exposures. Prominent bed boundaries are shown as horizontal lines. Lithofacies present include chert and laminated siltstone. Stratabound fractures are shown as horizontal lines. Lithofacies present include chert and laminated siltstone. Stratabound fractures are shown as horizontal lines. Lithofacies present include chert and laminated siltstone. Layer-cutting angled fractures are dashed and present in laminated siltstone. The image is oriented west to east.

Mapping results are from a sequence of interbedded chert and laminated siltstones (Figure 27). Two sets of fractures are noted in Vines Creek. Set one is oriented north-south. Set two is a conjugate set oriented northwest-southeast and northeast-southwest (Figure 28). The short planar fractures that appear perpendicular to the direction of the bedding are stratabound tensile fractures. These fractures occur in bedded chert or calcareous mudstones and are open. Layer-cutting angled fractures are also present as planar and restricted to laminated siltstone and organic-rich claystone lithofacies. Layer-cutting jagged fractures were also observed.

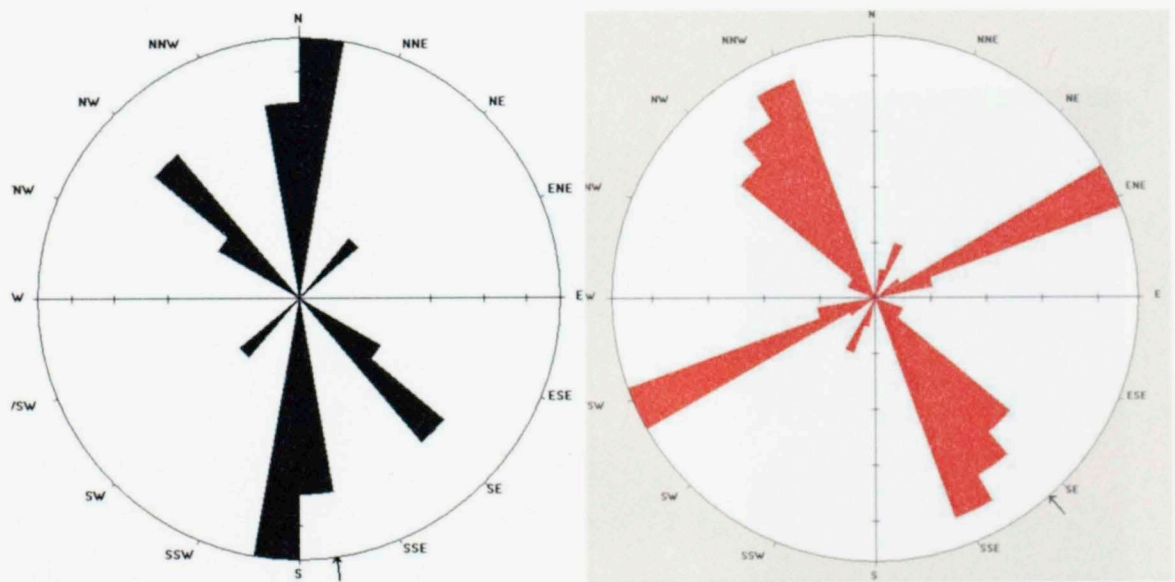


Figure 28 Vines Creek fracture directions.

Outcrop gamma-ray

The total Vines Creek section is 75 m thick (Figure 29) from the contact with the highest Hunton Limestone bed to the contact with the first Sycamore Limestone bed. Not all of the section is exposed, as some portions of the outcrop have been eroded and/or covered by soil and vegetation. The base of the section is poorly exposed at the Vines Creek outcrop and the outcrop gamma-ray is incomplete. However, where a measurement was obtained, the total gamma-ray matched high levels of Uranium and Potassium (Figure 30).

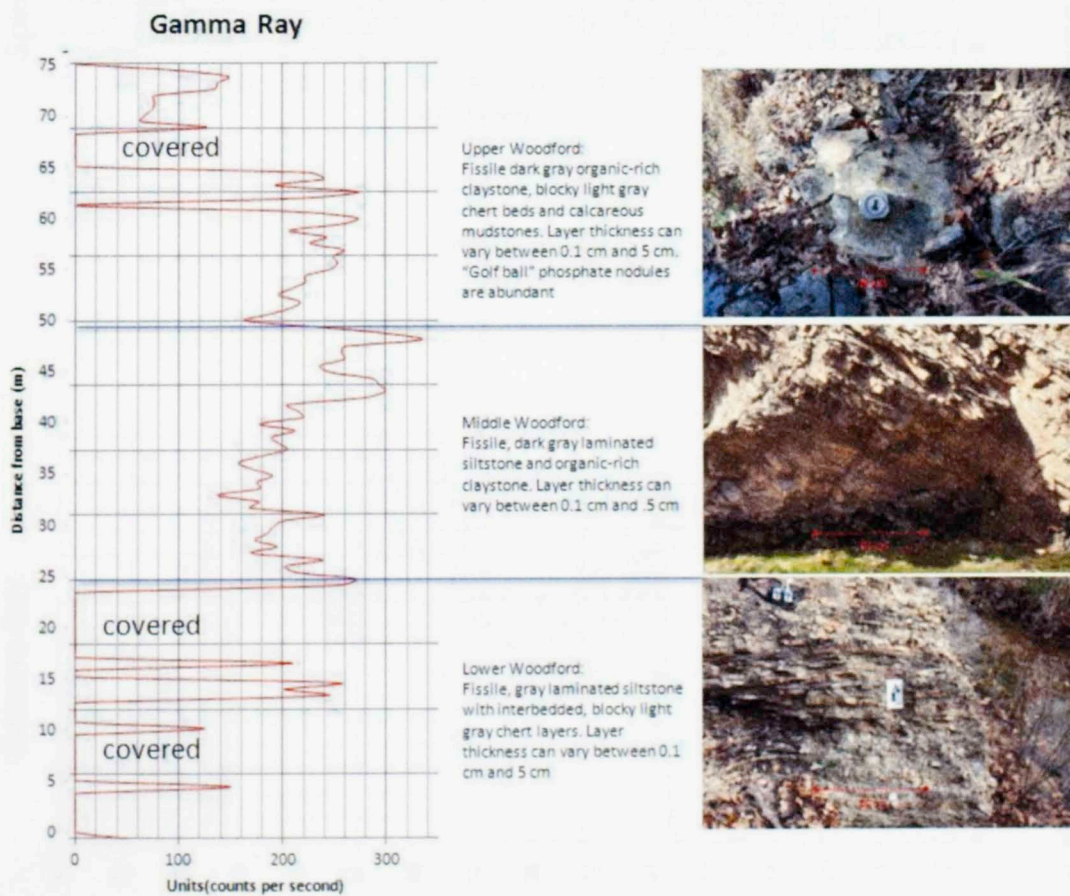


Figure 29 Vines Creek outcrop gamma-ray log, with typical rock characteristics.

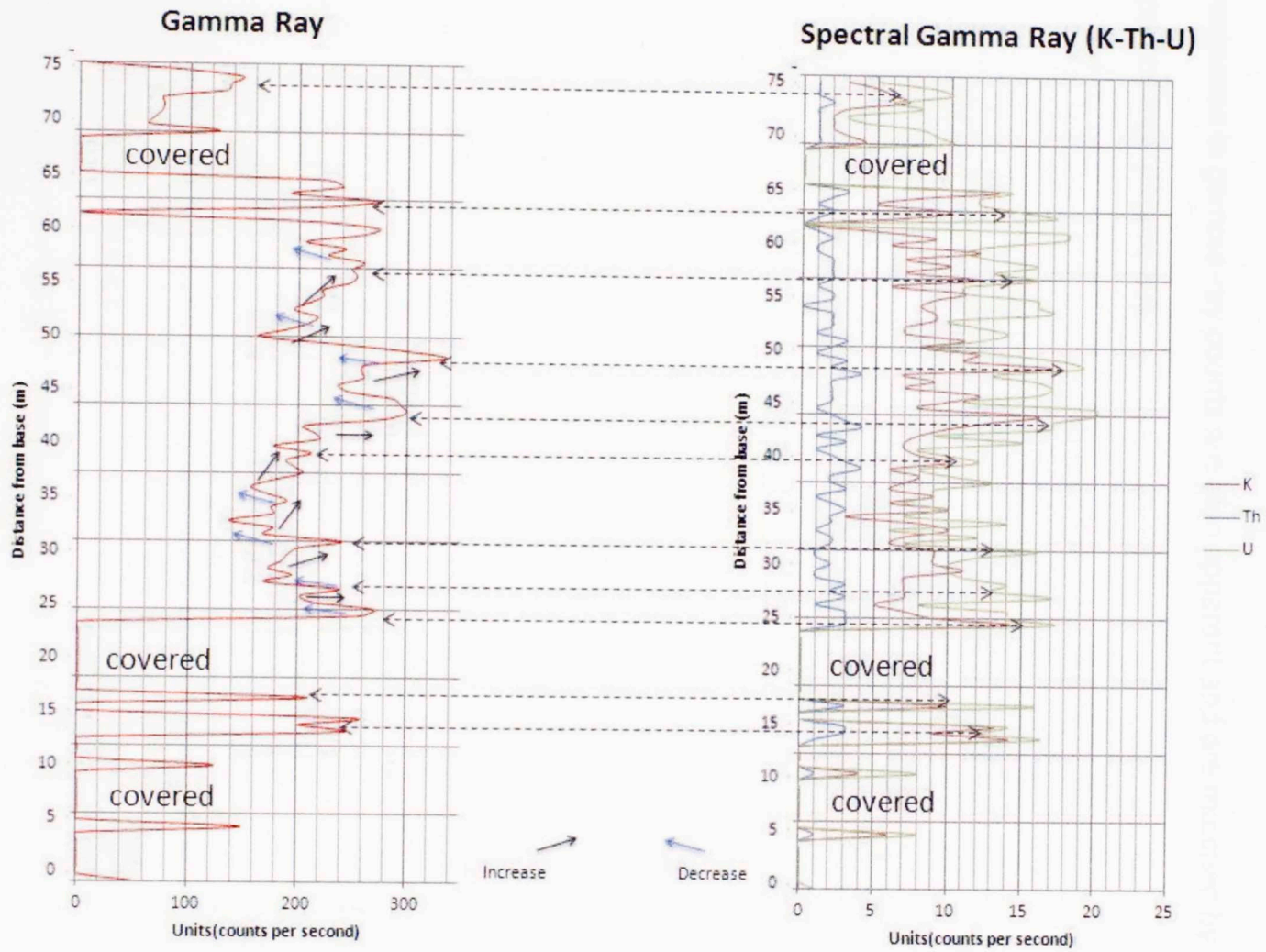


Figure 30 Vines Creek outcrop gamma-ray and spectral gamma-ray logs. Log patterns are highlighted.

3.2.4 Gamma-ray and spectral logs are relatively continuous between 25 and 60 m from the base. This continuous sequence exhibits an overall decrease in gamma-ray response, followed by a steep increase, shortly followed by a sharp decrease and then another increase near the top. Smaller increases and decreases in gamma-ray counts are also apparent and are matched by the spectral logs (Figure 30).

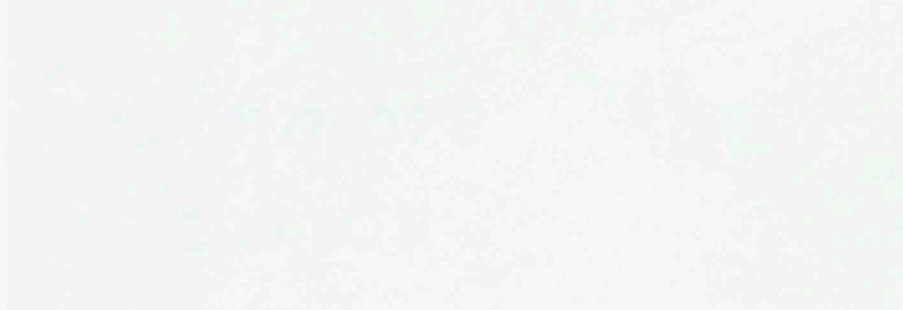


Figure 30. Gamma-ray and spectral logs (depth in meters).

The stratigraphic column is divided into several units (Figure 31). At the top, there is a thin layer of sandstone, followed by a layer of siltstone. The dominant feature is a thick, layered sequence of siltstone and sandstone. The stratigraphic column is marked by several distinct layers, including a layer of siltstone, a layer of sandstone, and a layer of siltstone. The stratigraphic column is marked by several distinct layers, including a layer of siltstone, a layer of sandstone, and a layer of siltstone. The stratigraphic column is marked by several distinct layers, including a layer of siltstone, a layer of sandstone, and a layer of siltstone.

Maps of layered sequences were constructed in a 2.5 m² survey area (Figure 32-34). The short, planar fractures are the stratigraphic units. The orientation of these fractures is north-south (Figure 32). The long, planar fractures are layer-cutting fractures. These fractures are oriented north-south between northwest and northeast. The spacing of all the fractures is approximately 100 m and appeared in three main directions.

3.2.4 Cool Creek (Lazy S Ranch)



Figure 31 Cool Creek Woodford Shale outcrop.

The stratigraphic sequence at Cool Creek is vertical (Figure 31). All five lithofacies are present, and fractures are present in all of them. The dominant fracture types present in this outcrop are stratabound and layer-cutting jagged. The stratabound planar joints are restricted to thickly bedded chert or calcareous mudstones. Some small faults were noted, cutting across many layers.

Maps of layered sequences were constructed in a 2.5 m² survey area (Figures 33-34). The short, planar fractures are the stratabound tensile fractures. The orientation of these fractures is north-south (Figure 32). The longer, jagged or semi-planar fractures are layer-cutting fractures. These fractures range in azimuth between northeast and northwest. The spacing for all the fractures mapped is not systematic and appeared to have a more clustered

distribution. Long lines perpendicular to the mapped fractures are interpreted layer boundaries (Figure 33).

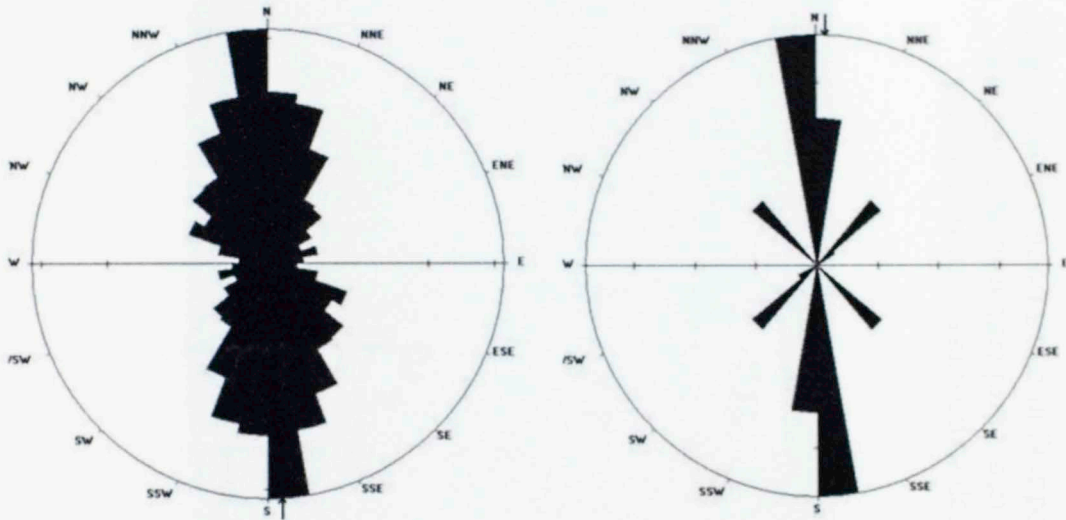


Figure 32 Cool Creek fracture orientations.

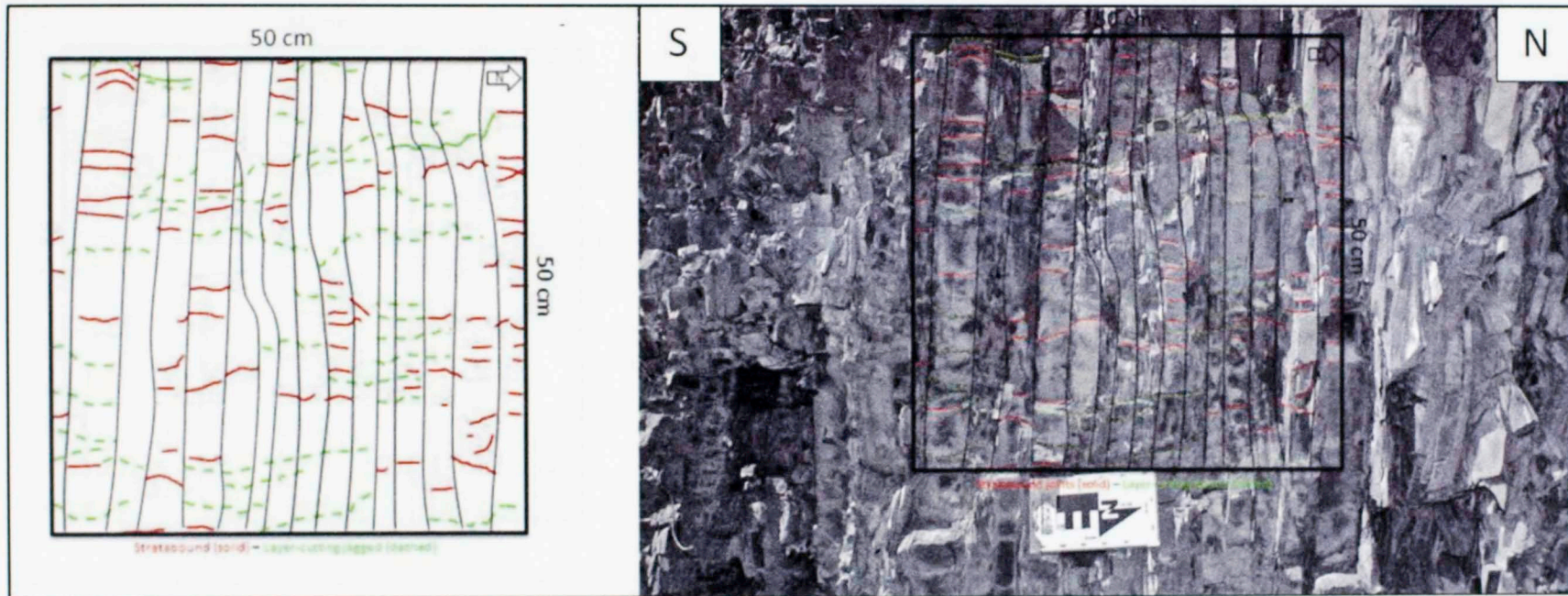


Figure 33 Cool Creek fracture survey square completed from outcrop exposures. Prominent bed boundaries are shown as vertical lines. Lithofacies present include chert and calcareous mudstone. Stratabound fractures are shown as short lines perpendicular to bedding in chert beds. Layer-cutting jagged fractures are dashed and cut across different lithofacies.

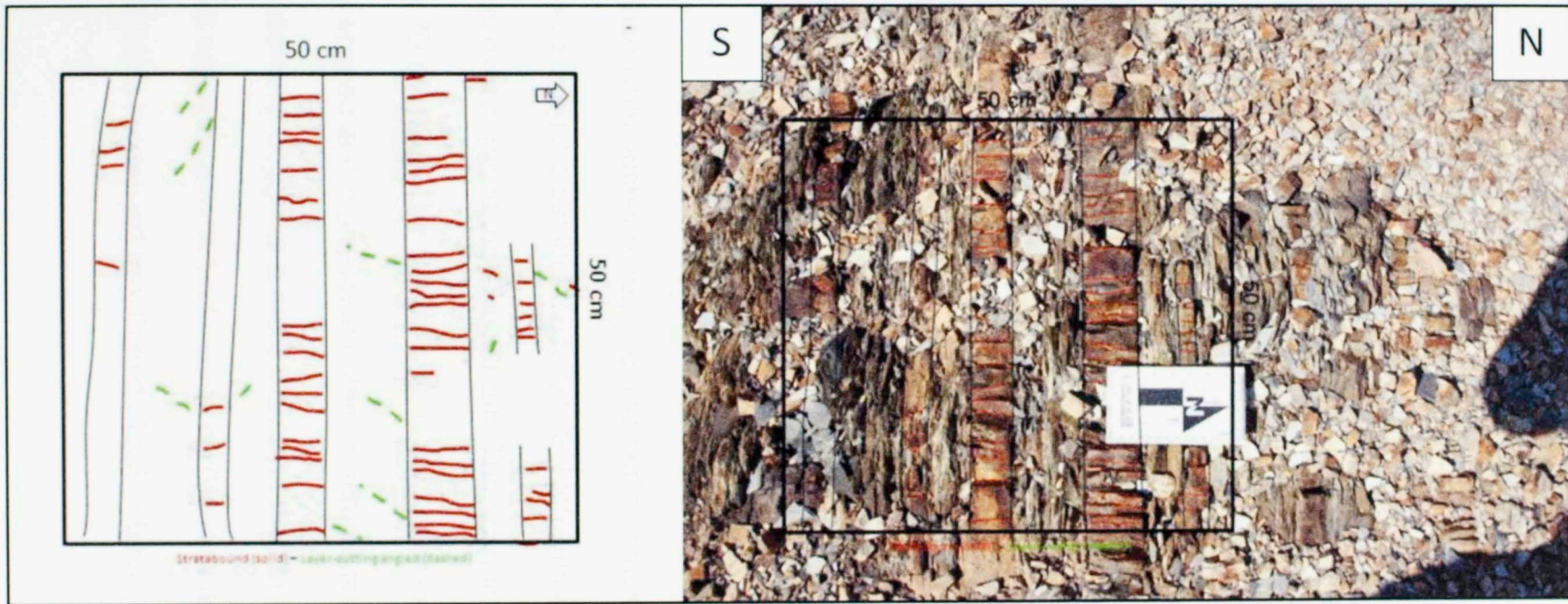


Figure 34 Cool Creek fracture survey square completed from outcrop exposure. Prominent bed boundaries are shown as vertical lines. Stratabound fractures are shown as short lines perpendicular to bedding. Layer-cutting fractures are dashed and angled to bedding.

Fracture statistics

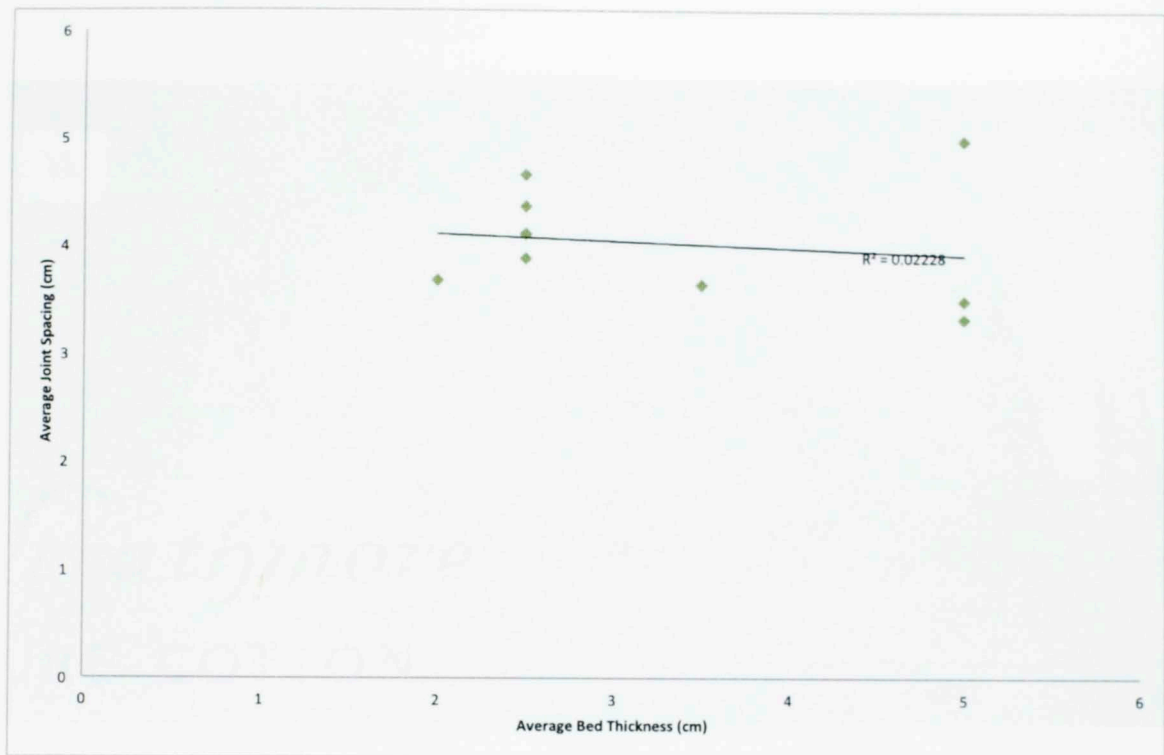


Figure 35 Cool Creek graphical relationship between bed thickness and fracture spacing.

The relationship between spacing and bed thickness (Figure 35) was obtained by measuring a scan line digitally with high-resolution images of several outcrop exposures along Cool Creek. The scan lines were approximately 70 cm long. The relationship is very poor as fractures are not systematically spaced and many layer-cutting fractures are present. Instead, the lack of relationship suggests a more clustered distribution. This observation is in agreement with the general understanding (Ladeira and Price, 1981) that thinner beds contain more fractures than do thicker beds.

3.2.5 Oklahoma Highway 77D



Figure 36 Oklahoma Highway 77D Woodford Shale outcrop of overturned beds, view is to the north.

The outcrop present along the north side of Oklahoma Highway 77D (Figure 36) has many good exposures of the Woodford Shale. The beds are overturned to the south and all of the lithofacies described are present along this outcrop. Most of the exposures are of bedding plane surfaces. All fracture types were observed, but layer-cutting angled fractures and faults are dominant.

Map results are shown in figure 38. The map is constructed from a bedding plane in a 2.5 m^2 survey square. The beds strike east-west and dip $70\text{-}80^\circ$ in a south-southwest direction. The short planar fractures that are parallel are the layer-cutting angled fractures. Four sets are present (Figure 37) with Set 1 oriented north-south, Set 2 oriented east-west, Set 3 oriented northeast-

southwest and Set 4 oriented east-northeast-west-southwest. The spacing for all the fractures is not systematic.

In a previous study by Ataman (2008), four sets with similar orientations were also observed at this location. He concluded that the high degree of deformation was a direct consequence of the overturning of the beds during the late stages of folding in the Arbuckle Mountains and that fracture distribution along an individual bed was controlled by the thickness and mechanical stratigraphy. Ataman (2008) also concluded that brittle layers contain more fractures.

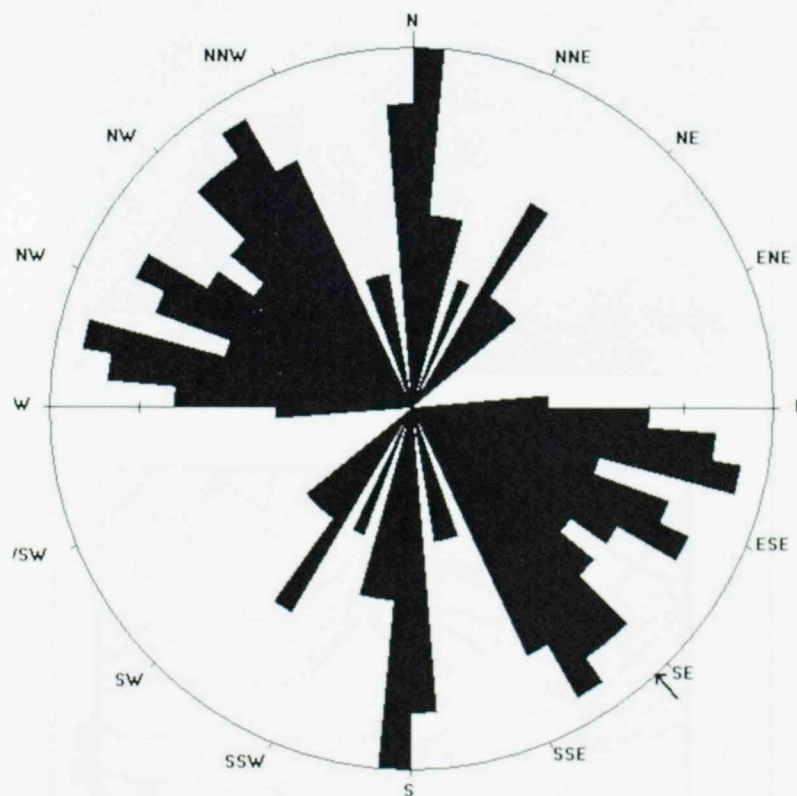


Figure 37 Oklahoma Highway 77D fracture orientations.

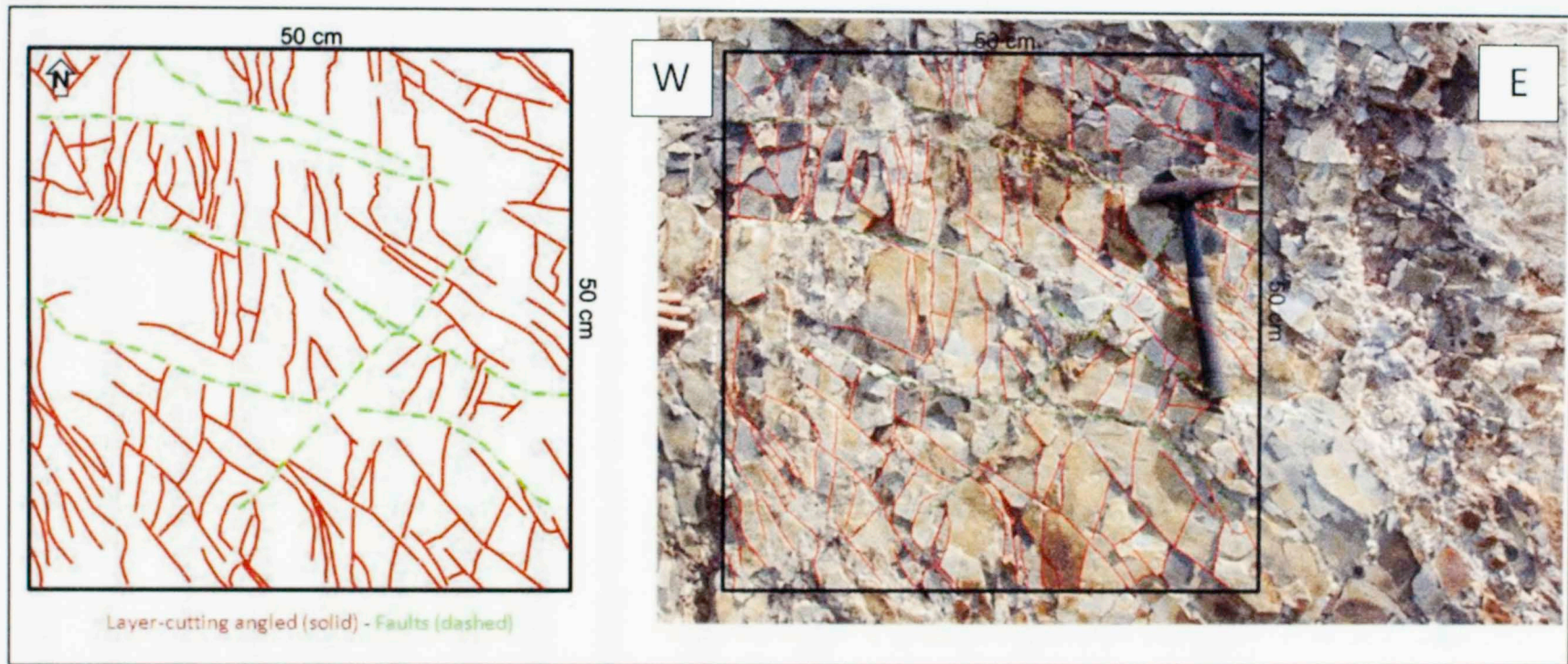


Figure 38 Oklahoma Highway 77D fracture survey square completed from outcrop exposures. Map constructed from laminated siltstone bedding plane shows layer-cutting angled fractures as short lines. Faults are dashed, segmented and offset other fractures. Clay gouge is present along the faults.

3.3 Discussion

3.3.1 Gamma-ray and sequence stratigraphy

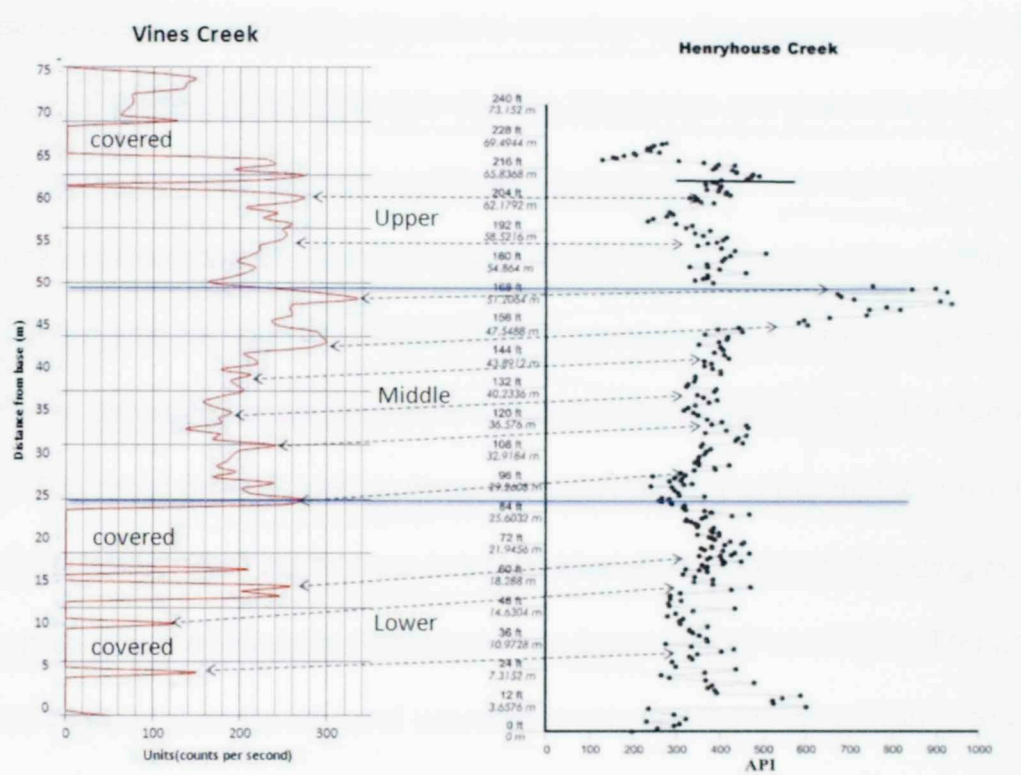


Figure 39 Vines Creek outcrop gamma-ray correlated with Henryhouse Creek Woodford Shale outcrop from Krystyniak (2006).

The gamma-ray log obtained in this study at Vines Creek correlates well with an outcrop gamma-ray log obtained by Krystyniak (2006) at the Henryhouse Creek outcrop (Figure 39). Therefore the Vines Creek exposure represents the lower, middle and upper Woodford Shale members (Lambert, 1993; Cardott, 2005). The gamma-ray log at Vines Creek is interpreted as a series of 3rd order sea level cycles superimposed on a 2nd order marine transgression (20-30 my). The sequence stratigraphic framework has been spliced together from rock type analysis, total and spectral gamma-ray logs, and correlations with previous studies (Cardot, 2005; Krystyniak, 2006; Paxton

et al., 2006; Micelli, 2010; Slatt et al., 2010). An upward increase in gamma-ray followed by a sharp decrease was interpreted as a 3rd order transgressive-regressive cycle. The middle Woodford member on the gamma-ray log contains at least 8 of these cycles. Coincidentally, the lithofacies are predominantly alternating sequences of chert and laminated siltstones. Several high gamma-ray peaks correspond to elevated levels of uranium and potassium in the spectral gamma-ray log. The high levels of uranium also suggest organic-rich sediments deposited in an anoxic or dysoxic depositional setting (Paxton et al., 2006). The most pronounced gamma-ray peak occurs at the middle-upper Woodford boundary. This marker is interpreted as a maximum flooding surface and represents the Devonian-Mississippian boundary (Over, 1992). The zone with the highest gamma-ray and uranium levels corresponds primarily to a sequence of organic-rich claystone. The upper Woodford also displays 3rd order sea level cycles with a major transgressive-regressive interval which correlates to high levels of uranium on the spectral gamma-ray log. The upper Woodford in outcrop also contains abundant phosphatic nodules. Other lithofacies present in the upper Woodford are calcareous mudstones, and laminated siltstones.

3.3.2 Fracture mapping

The fracture maps obtained at the study locations helped to create a spectrum of all the types of fractures present. The fracture types were then grouped together based on shape and relation to the lithology.

The most prominent fracture type is the stratabound fracture. This fracture type for the Woodford Shale can be defined as planar, mode I failure contained within a mechanical layer. Stratabound fractures are the primary failure mechanism of bedded chert and calcareous mudstones. The length of this type of fracture is directly proportional to the bed thickness. Joints that are bounded to a mechanical layer may add significant value as fracture porosity if they are open. However these fractures also appear to represent the earliest period of deformation, and may be present in the subsurface as mineralized veins, thereby lacking significant porosity. Nevertheless, mineralized stratabound fractures may also represent planes of weakness in the host rocks, which may decrease the strength of the layers.

Another common fracture type is the angled, layer-cutting fracture. This type of fracture occurs predominantly in laminated siltstone and organic-rich claystone lithofacies. This fracture is defined as layer cutting due to its tendency to traverse many laminations. This fracture is also inclined in respect to the bedding and often terminates at a mechanical layer boundary.

When a layer-cutting fracture occurs through a sequence that includes many different mechanical layers, the fracture type is defined as jagged. Jagged layer-cutting fractures are not associated with any one single rock type and can terminate abruptly at any one layer. However, the jagged shape appears to correlate with high frequency alternations of bedded chert and calcareous mudstone lithofacies. The shape reflects the mechanical differences and the change in orientation may be related to changing mechanical properties

across each boundary. A growth mechanism for this type of fracture is by the coalescence of stratabound and angled, layer-cutting fractures under intermediate to late-stage deformation. Layer-cutting jagged fractures may also represent an analog for the propagation of man-made hydraulic fractures. The extent of this fracture type is relevant as it can provide significant fracture permeability and connect isolated, brittle strata.

A less significant fracture type is the curved, mineralized or open fracture that develops in organic-rich claystone lithofacies. This fracture type usually is restricted to a few layers. Also, the curved shape of the fracture is a reflection of zones of weakness and stress concentration in sedimentary structures such as throughs, scour surfaces or ripples (Bahat et al., 2005). Curved fractures that are restricted to a few laminated claystone layers form in a similar manner as desiccation cracks in muddy sediments, but these could also be produced by thermal cracking of organic matter (Marquez and Mountjoy, 1996; Jarvie et al., 2007). This type of fracture can provide critical fracture porosity in lithofacies with extremely low matrix porosities.

Fracture swarms or clusters are long sections of many branching fractures. Swarms were commonly observed near faults and typically are zones of dense fracturing and intense deformation, which is difficult to quantify. Swarms are also long features that cut across many different mechanical layers. All other types of fractures may be present within a swarm to form this fracture type. Bitumen present in the Woodford Shale swarms indicates these zones of intense deformation were major conduits for migration of fluids.

Fracture swarms may also represent a true 'seismic scale' fracture that can be detected in three dimensions with seismic attributes such as coherence and curvature (Chopra and Marfurt, 2007). However, several aspects must be taken into consideration in order to comprehend the applicability of fracture clusters. Faults and swarms are closely related and can act as excellent flow paths for both hydrocarbons and water. Fracture clusters in outcrop also contain a significant amount of clay as a byproduct of the high density fracturing.

Shear fractures or faults are common in all of the outcrop locations in this study. This type of fracture most likely represents late stage deformation or a change in the regional stress regime. Large fractures coalesce to form long, continuous fracture zones that rotate and provide a mechanism for slip to occur. Smaller shear fractures are those that apparently began to slip when the stresses reach a certain threshold. All shear fractures contain a fine clay gouge in the fault zone which would likely act as a flow baffle or barrier. In some exposed fault planes, slickenlines are present, which indicate the direction of displacement or slip. Small strike-slip and dip-slip faults are present in all outcrops.

3.3.3 Fractures and mechanical stratigraphy

The current maximum horizontal stress orientation in the Arbuckle Mountains is roughly oriented northeast-southwest. The dominant stratabound fracture orientation is north-south. Stratabound fractures are likely remnants of early stage deformation and tensile failure during burial and pore-pressure

increase. Layer-cutting, angled fractures are oriented northwest-southeast and northeast-southwest. These orientations also reflect a paleostress field, although the second set is closer to the current stress field, which indicates an episode of late stage deformation.

Understanding the relationship between the brittle-ductile couplet and the fracture type is one of the primary goals of this study. The brittle-ductile couplet is observed in outcrop and in experiment Setup 3 and 4 as a brittle layer between two ductile layers. The brittle parts in the Woodford are the cherts and the calcareous mudstones. The ductile parts are laminated siltstones and organic claystones. The unit or couplet is assumed compacted. The ductile layers distribute the loading to the brittle layer and also help to isolate a single brittle bed from the shadow effect of other nearby fractures (McConaughy and Engelder, 2001).

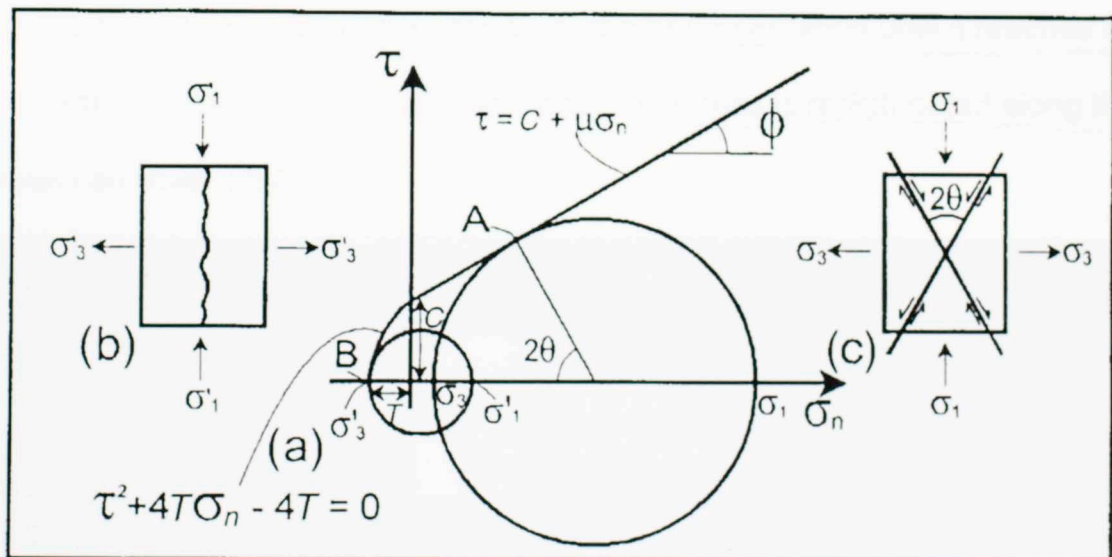


Figure 40 Failure mode relationships to principal stresses (Cosgrove, 2001).

Since the different mechanical layers are acting as a coupled unit, as it deforms, all layers undergo the same amount of deformation (Gross and Engelder, 1995). However, the differences in mechanical properties result in each mechanical layer behaving differently. The ductile layers first extend and change in length without failure. The shear stress is transferred to the brittle layer in the middle of the couplet by a process known as the Cox-Hobbs case (Cox, 1951, Hobbs, 1967, Gross et al. 1995). Under the Griffith criteria the stress is accumulated around a flaw until the applied stress overcomes the tensile strength of the material (Figure 40). Due the stress being transferred to the brittle layer, via the ductile layers, failure begins to occur at the interface of the two mechanical units. Once the first crack forms it relaxes the stresses in a shadow zone around it, and stress accumulates at another point in the material where it will form a new crack (Figure 41).

The fracture propagates perpendicular to the bed orientation until it reaches the next brittle-ductile boundary, at which point the stress is redistributed along the contact as shear stress.

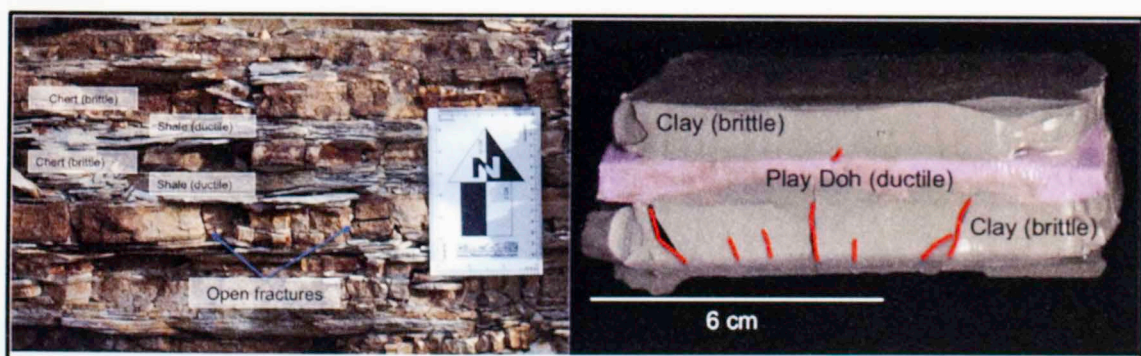


Figure 41 Comparison of typical Woodford Shale outcrop section and results from Setup 3 analog modeling of brittle-ductile couplets.

In the field, layer-cutting angled fractures are very common. The mechanism for the development of this type of fracture can be explained as a continuation of the aforementioned process of joint initiation in a brittle-ductile couplet. The process would include brittle deformation in the 'ductile' layer with increasing deformation, or by conditions under which a 'ductile' layer becomes stiffer and mechanically 'brittle'. Such conditions include deep burial, dewatering or thermal maturation (Cosgrove, 2001).

As a fracture propagates through the brittle layer, and the stress front encounters the brittle-ductile boundary, the stress becomes shear and moves parallel to the boundary until it encounters a flaw in the laminated, ductile, layer (Hobbs, 1967; Gross et al., 1995; Bahat et al., 2005). The result is a shear fracture that propagates at an angle (internal angle of friction per Coulomb criteria) and cuts across the mechanical layer thickness of the laminated

interval. This coincides with the many layer-cutting fractures observed in thinly laminated claystones and siltstones.

3.3.4 Application for drilling and completion

The correlation between gamma-ray stacking patterns and spectral gamma-ray logs is a powerful tool for predicting brittle and ductile lithofacies (Slatt and Abousleiman, 2011). The more brittle lithofacies of the Woodford Shale occur along intervals of lower gamma-ray, uranium, and thorium. Ductile lithofacies are characterized by high gamma-ray and high uranium content. The gamma-ray stacking patterns also seem to discriminate the failure type of the

formation, which is lithologically controlled (Gross, 1993; Gross et al., 1995; Ataman, 2008; Busetti, 2009). Low gamma-ray sections are likely to undergo tensile failure as the primary mode. High gamma-ray sections may undergo shear failure.

The predictability of mechanical stratigraphy and failure modes can be applied to drilling by planning lateral well placement with more accuracy. Furthermore, the characterization of the stress field from borehole breakouts would provide the optimal orientation for drilling and hydraulic fracture stimulations. Zones of more brittle rocks can be accessed from the gamma-ray stacking patterns and become primary landing targets for horizontal wells. As described in outcrop, these zones should contain abundant natural tensile fractures that may or may not be healed. Furthermore, brittle zones are less likely to be clay rich which should mitigate clay swelling by drilling fluids. Because natural fractures are representative of major zones of weakness, they can be exploited by drilling perpendicular to the major set. Zones of more ductile rocks can be accessed from sections of high gamma-ray and uranium as described from the outcrop locations. These zones would act as fracture barriers as predicted by the analog modeling conducted in this study. The fracture may stop at major mechanical boundaries, or become redistributed as bed-parallel shear fractures. Also, because these zones are more likely to be dominated by clay-rich rocks, they should be avoided for horizontal well placement as they can have swelling clays and present drilling hazards.

Analog experiments have also demonstrated that bedding plane contacts for the Woodford Shale may be significant planes of weakness. The correct recognition of a major mechanical boundary can also be used as a hydraulic fracture stimulation target. When applicable by the local stress field, a bed parallel stimulation can be more effective at exploiting the formation's natural weakness.

Overall total gamma-ray and spectral gamma-ray, coupled with outcrop characterization efforts should be used to create more detailed drilling and completion targets for horizontal wells by recognizing and exploiting weaker portions of the formation.

4. CONCLUSIONS

The Woodford Shale is well exposed in the Arbuckle Mountains of southeast Oklahoma. The outcrops in this study were characterized in terms of lithofacies, and fractures. Additionally, a nearly complete section of the Woodford Shale at Vines Creek was characterized with outcrop gamma-ray and spectral gamma-ray logs.

The Woodford Shale sequence is representative of a 2nd order marine transgression. Higher frequency 3rd order sea level cycles could be inferred from gamma-ray and spectral gamma-ray patterns. The gamma-ray peaks correlated well with high levels of uranium. This would suggest a depositional setting with low levels of sedimentation in which quiet and dysoxic water aided in the preservation of organic matter.

Outcrop lithofacies also suggest a siliciclastic marine system as the depositional setting. The frequent transitions from bedded chert to laminated siltstone suggest changes in the depositional environment from high to low energy and variations in productivity. Phosphatic-rich zones can be indicative of upwelling zones or low sedimentation rates in anoxic to dysoxic conditions; however, because phosphatic-rich zones also correlate with intervals of high gamma-ray, the latter interpretation might be more relevant. Finely laminated, organic rich mudstones also correlate with high levels of uranium and total gamma-ray, also suggesting low sedimentation rates and dysoxia which aided in the preservation of the organic matter.

The stratigraphy is directly related to the mechanical properties of the Woodford Shale. Although the overall composition of the formation is high in siliciclastics, making the mechanical stratigraphy dominantly brittle, laminated siltstones and organic-rich claystones appear to be more ductile. This makes the Woodford Shale a vertically anisotropic material that breaks and deforms under stress in different ways across each layer.

The fracture patterns described from outcrop revealed that chert and calcareous mudstones are brittle and contain abundant stratabound tensile fractures. This type of fracture is very common throughout the Woodford Shale and could be representative of the earliest stages of deformation. Another common type of fracture is a layer-cutting angled set that typically occurs in laminated siltstones and organic-rich claystone facies. This fracture type indicates these layers failed under very high stresses or deep in the subsurface. Another type of layer-crossing fracture is also present in outcrop cross-cutting many different lithofacies as jagged or en-echelon segments. This fracture type is relevant and might represent the way in which strata-bound and layer-crossing fractures are connected under late-stage deformation. Fracture swarms were also noted in close proximity to faults. These zones of high fracture density are often branching and filled with bitumen and are indicative of high levels of deformation and fluid flow.

A set of analog models were created using wet clay and Play-Doh to represent brittle and ductile layers and extended to create tensile fractures. The models demonstrated the mechanism by which the observed fracture patterns

likely formed. Tensile fractures nucleated at the contact of the two different experiment materials, then propagated perpendicular to the layers but did not propagate through the ductile layers. The analog experiments also demonstrated that the layer boundary is also a very weak surface prone to failure under low levels of stress.

5. RECOMMENDATIONS

1. Characterize Woodford Shale fractures from borehole image logs and core to correlate with outcrop fracture studies.
2. Conduct finite element modeling of a multilayered sequence with Woodford Shale parameters.
3. Characterize fractures from other prominent shale formations in outcrop to obtain further insight into other deformation styles.
4. Correlate sequence stratigraphy stacking patterns from total gamma-ray and spectral gamma-ray with detailed measured sections to improve on predictability of brittle and ductile rocks.
5. Develop a 3D reservoir model for the Woodford Shale Wyche Quarry in the Arbuckle Mountains, and apply known parameters to test optimal drilling plans.
6. Develop a calibration mechanism between gamma-ray stacking patterns and estimated fracture densities per interval.

REFERENCES

- Ataman, O., 2008, Natural fracture systems in the Woodford Shale, Arbuckle Mountains, Oklahoma: Master's thesis, Oklahoma State University, Stillwater, Oklahoma, 158 p.
- Anderson, E. M., 1951, The dynamics of faulting, Oliver and Boyd, White Plains, New York, 206 p.
- Baer, G., 1991, Mechanisms of dike propagation in layered rocks in massive porous sedimentary rocks: *Journal of Geophysical Research*, v. 96-b7, p. 11911-11929.
- Baer, G., Reches, Z., 1991, Mechanisms of emplacement and tectonic implications of the Ramon dike systems, Israel: *Journal of Geophysical Research*, v. 96-b7, p. 11895-11910.
- Bahat, D., Rabinovitch, A., Frid V., 2005, Tensile fracturing in rocks: Springer, Berlin, 569 p.
- Bai, T., and Pollard, D., 2000, Fracture spacing in layered rocks: a new explanation based on the stress transition: *Journal of Structural Geology*, v. 22, p. 43-57.
- Becker, A., Gross, M.R., 1996, Mechanism for joint saturation in mechanically layered rocks: an example from southern Israel: *Tectonophysics*, v. 257, p. 223-237.
- Bergbauer, S., Pollard, D., 2004, A new conceptual fold-fracture model including prefolding joints, based on the Emigrant Gap anticline, Wyoming: *GSA Bulletin*, v. 116, p. 294-307.
- Busetti, S., 2009, Fracturing in layered reservoir rocks: PhD thesis, University of Oklahoma, Norman, Oklahoma, 256 p.

Cardott, B.J., and M.W. Lambert, 1985, Thermal maturation by vitrinite reflectance of Woodford Shale, Anadarko basin, Oklahoma: AAPG Bulletin, v. 69, p. 1982-1998.

Cardott, B.J., 2005, Overview of unconventional energy resources of Oklahoma, *in* B.J. Cardott, ed., Unconventional energy resources in the southern Midcontinent, 2004 symposium: Oklahoma Geological Survey Circular 110, p. 7-18.

Chopra, S., and Marfurt, K. J., 2007. Seismic attributes for prospect identification and reservoir characterization: Geophysical Developments, no. 11, Society of Exploration Geophysicists, Tulsa, 464 p.

Comer, J.B., and Hinch, H.H., 1987, Recognizing and quantifying expulsion of oil from the Woodford Shale and age-equivalent rocks in Oklahoma and Arkansas: AAPG Bulletin, v. 71, p. 844-858.

Comer, J.B., 2005, Facies distribution and hydrocarbon production potential of Woodford Shale in the southern Midcontinent, *in* B.J. Cardott, ed., Unconventional energy resources in the southern Midcontinent, 2004 symposium: Oklahoma Geological Survey Circular 110, p. 51-62.

Cosgrove, J.W., 1995, The expression of hydraulic fracturing in rocks and sediments, *in* M.S. Ameen, ed., Fractography: fracture topography as a tool in fracture mechanics and stress analysis: Geological Society Special Publication, v. 92, p. 187-196.

Cosgrove, J.W., 2001, Hydraulic fracturing during the formation and deformation of a basin: A factor in the dewatering of low-permeability sediments: AAPG Bulletin, v. 85-4, p. 737-748.

Cox, H., 1951, The elasticity and strength of paper and other fibrous material: British Journal of Applied Physics, v. 3, p. 72-79.

Engelder, T., 1987, Joints and shear fractures in rocks: *in* Atkinson, B., Fracture Mechanics of Rocks: Academic Press, London, 551 p.

Fay, R.O., 1989, Geology of the Arbuckle Mountains along Interstate 35, Carter and Murray Counties, Oklahoma: Oklahoma Geological Survey Guidebook 26, 50 p.

Germanovich, L.N., Dyskin, A.V., 2000, Fracture mechanisms and instability of openings in compression: International Journal of Rock Mechanics and Mining Sciences, v. 37, p. 263-284.

Germanovich, L.N., Salganik, R.L., Dyskin, A.V., Lee, K.K., 1994, Mechanisms of brittle fracture of rock with pre-existing cracks in compression: PAGEOPH, v. 143, p. 117-149.

Granath, J.W., 1989, Structural evolution of the Ardmore Basin, Oklahoma: progressive deformation in the foreland of the Ouachita collision: Tectonics, v. 8-5, p. 1015-1036.

Griffith, A., 1921, The phenomena of rupture and flow in solids: *in* Philosophical Transactions of the Royal Society of London. Series A, Containing Papers of a Mathematical or Physical Character, v. 221, p. 163-198.

Gross, M., 1993, The origin and spacing of cross joints: examples from the Monterey Formation, Santa Barbara coastline, California: Journal of Structural Geology, v. 15-6, p. 737-751.

Gross, M., 1995, Fracture partitioning: failure more as a function of lithology in the Monterey Formation of coastal California: GSA Bulletin, v. 107-7, p. 779-792.

Gross, M., Fischer, M., Engelder, T., Greenfield, R., 1995, Factors controlling joint spacing in interbedded sedimentary rocks: integrating numerical models with field observations from the Monterey Formation, USA: *in* M.S. Ameen, ed., Fractography: fracture topography as a tool in fracture mechanics and stress analysis: Geological Society Special Publication, v. 92, p. 215-233.

Ham, W.E., 1951, Structural geology of the southern Arbuckle: Tulsa Geological Society Digest, v. 19, p. 68 – 72.

Ham, W.E., Dennison, R.E., and Merritt, C.A., 1964, Basement rocks and structural evolution of southern Oklahoma: Oklahoma Geological Survey Bulletin 95, 302 p.

Ham, W.E., 1969, Regional geology of the Arbuckle Mountain region: Oklahoma Geological Survey Guidebook 17, 52 p.

Ham, W.E., and others, 1973, Regional geology of the Arbuckle Mountains, Oklahoma: Oklahoma Geological Survey Special Publication 73-3, 61 p.

Hester, T.C., J.W. Schmoker, and H.L. Sahl, 1990, Log-derived regional source-rock characteristics of the Woodford Shale, Anadarko basin, Oklahoma: U.S. Geological Survey Bulletin 1866-D, 38 p.

Heidbach, O., Tingay, M., Barth, A., Reinecker, J., Kurfeß, D., and Müller, B., 2008, The World Stress Map database release 2008
doi:10.1594/GFZ.WSM.Rel2008

Hudson, J. A., Liu, E. and Crampin, S., 1996, The mechanical properties of materials with interconnected cracks and pores: *Geophysical Journal International*, v. 124, p.105–112.

Jarvie, D. M., R. J. Hill, T. E. Ruble, and R. M. Pollastro, 2007, Unconventional shale gas systems: the Mississippian Barnett Shale of north central Texas as one model for thermogenic shale gas assessment: *in* R.J. Hill and D.M. Jarvie, eds., Barnett Shale: AAPG Bulletin Special Issue, v. 90, no. 4, p. 475- 499.

Krystyniak, A.M., 2006, Outcrop-based gamma-ray characterization of the Woodford Shale of south-central Oklahoma: Stillwater, OK, Oklahoma State University, unpublished M.S. thesis, 145 p.

Ladeira, F.L., Price, N.J., 1981, Relationship between fracture spacing and bed thickness: *Journal of Structural Geology*, v. 3-2, p. 179-183

Lambert, M.W., 1993, Internal stratigraphy and organic facies of the Devonian-Mississippian Chattanooga (Woodford) Shale in Oklahoma and Kansas, *in* B.J.

Katz and L.M. Pratt, eds., Source rocks in a sequence stratigraphic framework: AAPG Studies in Geology 37, p. 163-176

Lash, G., Loewy, S., Engelder, T., 2004, Preferential jointing of Upper Devonian black shale, Appalachian Plateau, USA: evidence supporting hydrocarbon generation as a joint-driving mechanism: *in* J.W. Cosgrove & T. Engelder, eds, The initiation, propagation and arrest of joints and other fractures, Geological Society, London, Special Publications, v. 231, p. 129-151.

Lockner, D. A., Moore, D. E., and Reches, Z., 1992, Microcrack interaction leading to shear fracture, *in* J.R. Tillerson, and W.R. Wawersik, eds., Proceedings of the 33rd U.S. Symposium on Rock Mechanics: Rotterdam, Netherlands, Balkema, p. 807-816.

Lorenz, J.C., Teufel, L.W., Warpinski, R., 1991, Regional fractures I: a mechanism for the formation of regional fractures at depth in flat-lying reservoirs: AAPG Bulletin, v. 75-11, p. 1714-1737.

Lorenz, J.C., Finley, J., 1991, Regional fractures II: fracturing of Mesaverde reservoirs in the Piceance Basin, Colorado: AAPG Bulletin, v. 75-11, p. 1738-1757.

Marquez, X., Mountjoy, E., 1996, Microfractures Due to Overpressures Caused by Thermal Cracking in Well-Sealed Upper Devonian Reservoirs, Deep Alberta Basin: AAPG Bulletin, v. 80-4, p. 570-588.

McConaughy, D., Engelder, T., 2001, Joint initiation in bedded clastic rocks: Journal of Structural Geology, v. 23, p. 203-221.

Miceli, A., 2010, Geochemical Characterization of the Woodford Shale, Southeastern Oklahoma: Master's thesis, University of Oklahoma, Norman, Oklahoma, 132 p.

Over, D.J., and J.E. Barrick, 1990, The Devonian/Carboniferous boundary in the Woodford Shale, Lawrence uplift, south-central Oklahoma, *in* S.M. Ritter, ed., Early to middle Paleozoic conodont biostratigraphy of the Arbuckle Mountains, southern Oklahoma: OGS Guidebook 27, p. 63-73.

Over, D.J., 1992, Conodonts and the Devonian-Carboniferous boundary in the upper Woodford Shale, Arbuckle Mountains, south-central Oklahoma: *Journal of Paleontology*, v. 66, p. 293-311

Paxton, S., Cruse, A., Krystyniak, A., 2006, Detailed Fingerprints of Global Sea-level Change Revealed in Upper Devonian / Mississippian Woodford Shale of South-Central Oklahoma: AAPG Search and Discovery *presented at AAPG Annual Convention*, Houston, Texas, April 9-12, 2006

Portas Arroyal, R.M., 2009, Characterization and origin of fracture patterns in the Woodford Shale in southeastern Oklahoma for application to exploration and development: Master's thesis, University of Oklahoma, Norman, Oklahoma, 110 p.

Randel, C., 2008, Structure and chronology of the Washita Valley Fault, Southern Oklahoma Aulacogen: *Shale Shaker*, v.39, p. 2-13.

Reches, Z., 1983, Faulting of rocks in three-dimensional strain field, II, Theoretical analysis: *Tectonophysics*, v. 95, p. 133-156.

Rives, T., Rawnsley, K.D., Petit, J.P., 1994, Analogue simulation of natural orthogonal joint set formation in brittle varnish: *Journal of Structural Geology*, v.16-3, p. 419-429.

Saggy, A., Reches, Z., Agnon, A., 2003, Hierarchic three-dimensional structure and slip partitioning in the western Dead Sea pull-apart: *Tectonics*, v. 22-1, p. 1-17.

Sierra, R., Tran, M.H., Abousleiman, Y.N., Slatt, R.M., 2010, Woodford Shale Mechanical Properties and the Impacts of Lithofacies: ARMA paper 10-461 *presented at 44th US Rock Mechanics Symposium and 5th U.S.-Canada Rock Mechanics Symposium*, Salt Lake City, June 27-30, 2010.

Slatt, R.M., J.M. Borer, B.W. Horn, H.A. Al-Siyabi, and S.R. Pietraszek, 1995, Outcrop gamma-ray logging applied to subsurface petroleum geology, *Mountain Geologist*, v. 32, p. 81-94.

Slatt, R.M., Portas, R., Buckner, N., Abousleiman, Y., O'Brien, N., Tran, M., Sierra, R., Philp, P., Miceli-Romero, A., Davis, R., Wawrzyniec, T., 2010, Outcrop/behind outcrop (quarry), multiscale characterization of the Woodford gas shale, Oklahoma: *in press*

Slatt, R., Abousleiman, Y., 2011, Merging sequence stratigraphy and geomechanics for unconventional gas shales: *The Leading Edge*, v. 30-3, p. 274-282.

Sullivan, K. L., 1985, Organic facies variation of the Woodford Shale in western Oklahoma: *Shale Shaker*, v. 35, p. 76-89.

Suneson, N. H., 1997, The geology of the eastern Arbuckle Mountains in Pontotoc and Johnston counties, Oklahoma – An introduction and field-trip guide: Oklahoma Geological Survey Open File Report 4-97.

Wu, H., and Pollard, D., 1995, An experimental study of the relationship between joint spacing and layer thickness: *Journal of Structural Geology*, v. 17-6, p. 887-905.